Construction and Building Materials 400 (2023) 132606

Contents lists available at ScienceDirect

Construction and Building Materials

journal homepage: www.elsevier.com/locate/conbuildmat

Artificial intelligence-based prediction of strengths of slag-ash-based geopolymer concrete using deep neural networks

Solomon Oyebisi [a,*], Thamer Alomayri [b]

[a] Department of Civil Engineering, Covenant University, PMB 1023, Km 10, Idiroko Road, Ota, Nigeria
[b] Department of Physics, Faculty of Applied Science, Umm Al-Qura University, 21955, Makkah, Saudi Arabia

ARTICLE INFO

Keywords:
Alkali
Artificial intelligence
Ash
Compressive strength
Geopolymer concrete
Sustainable production

ABSTRACT

The construction and building industry, one of the greatest emitters of greenhouse gases, is under tremendous pressure because of the growing concern about global climate change and its detrimental effects on societies. Given the environmental problems connected to cement production, geopolymer concrete has become a viable alternative. In addition, if the concrete strength results failed to meet the specified strength after being cast, modifications are impossible. Thus, it is particularly desirable to predict strength prior to casting concrete. This study presents the first effort in applying deep neural networks (DNN) of AI techniques to predict the mechanical strengths (GGBFS) of geopolymer concrete (GPC) produced from corncob ash and ground granulated blast furnace slag. The mixes were activated with 12–16 M of alkali solutions at ambiently cured conditions for 7–90 days. Following that, back propagation learning algorithms were created for forecasting the concrete strengths based on concrete mix proportions. The mechanical strengths estimated by the DNN were verified by laboratory testing results. Results revealed that GGBFS, mix grade, curing days, and alkali precursor are variables that govern the mechanical strengths of the GGBFS-CCA-GPC. Forecasting the mechanical properties of GPC produced using DNN shows that the relationship between the input and output arguments could be most accurately predicted by a 10–20–20–20-1 network topology, evident by approximately 99% correlation coefficient between the actual and predictive values for compressive and flexural strengths. However, the 10–17–17–17-1 network architecture showed the best DNN for predicting split tensile strength, with a 97% correlation coefficient between the actual and projected values. This study demonstrated that the DNN techniques are efficient in predicting the mechanical strengths of GPC based on the mix proportions. Application of these techniques will greatly advance concrete quality assurance.

1. Introduction

Through the ages, there has been an increasing awareness of the environmental impact of concrete's dominance as a key building material [1]. Because of the expanding population, there is a higher need for raw materials. According to projections, the global cement and concrete market would have doubled by 2050, increasing carbon emissions and harming biodiversity [2]. Portland cement (PC) production requires a large amount of energy and has a large carbon footprint; research has focused on developing alternative binders [2]. Portland cement, the primary binding component of concrete, requires about 1.7 tons of raw materials to produce, which results in the atmospheric release of about 0.8 tons of carbon dioxide [3]. These circumstances necessitate quick action to mitigate the negative effects of cement manufacturing on climate change [2]. Recycling agricultural and industrial wastes with natural compositions and origins to create building materials is one of the scientific and technological ways to achieve material sustainability [4]. Recycling agricultural and industrial waste materials as supplemental cementitious materials (SCMs) has positive effects on the environment, the economy, and the society [5,6]. It has been demonstrated that replacing PC with waste materials is a workable, affordable, and environmentally responsible way to reduce carbon footprint [7–9]. Even in radiation shielding, replacing PC with other materials has indicated to increase the effectiveness of the environment's protection from dangerous radiation [9–11].

The fact that the PC has been completely removed from the mixture and substituted with other ingredients like recycled agro-industrial materials is a key characteristic of geopolymer concrete (GPC), a type

* Corresponding author.
E-mail addresses: solomon.oyebisi@covenantuniversity.edu.ng (S. Oyebisi), tsomayri@uqu.edu.sa (T. Alomayri).

https://doi.org/10.1016/j.conbuildmat.2023.132606
Received 26 June 2023; Received in revised form 20 July 2023; Accepted 23 July 2023
Available online 3 August 2023

Table 1
Several ML techniques of AI-based system in predicting concrete properties.

S/N	Algorithm	Input	Output	Dataset	Reference
1	ANN	PC, curing age, water, aggregates, and micro air	CS	144	[76]
2	ANN	PC, GGBFS, SP, aggregates, water, and sample age	CS	225	[77]
3	ANN	PC, SF, water content, aggregates; SP, and sample age	CS	240	[78]
4	ANN	FAS, NaOH solution, Na_2SiO_3 gel, and water	CS	210	[79]
5	ANN	Sample age; NaOH concentration, NZ, SF; GGBFS	CS	117	[18]
6	ANN	PC, GGBFS, FAS, SP, aggregates, water, and sample age	CS	300	[80]
7	ANN	GGBFS, FAS, SP, aggregates, water, and sample age	CS	1133	[81]
8	ANN	PC, GGBFS, FAS, SP, aggregates, water, and sample age	TS	1133	[81]
9	ANN	GGBFS, FAS, SP, aggregates, water, and sample age	CS	2817	[78]
10	ANN	Water/solid ratio, Alkaline activator/binder ratio, Na-Silicate/NaOH ratio, FAS/GGBFS ratio, and NaOH molarity	CS	1030	[82]
11	DT	PC, GGBFS, FAS, SF, aggregates, water, and sample age	CS	40	[83]
12	DT	PC, curing age, water, aggregates, and micro air	CS	144	[76]
13	RT	Water/binder ratio, GGBFS/water ratio, FAS/water ratio, coarse aggregate/binder ratio, and coarse aggregate/fine aggregate ratio	CS	1030	[84]
14	DT	PC, GGBFS, FAS, SP, aggregates, water, and sample age	CS	300	[80]
15	DT	PC, GGBFS, FAS, SP, aggregates, water, and sample age	CS	1030	[85]
16	DT	PC, GGBFS, FAS, SP, aggregates, water, and sample age	CS	1030	[86]
17	SVM, GPR	RHA, FAS, curing time, and temperature	CS	70	[87]
18	SVM, GEP	GGBFS, FAS, SP, NaOH and KOH solutions, Na_2SiO_3 gel, aggregates, water, oven-cured and ambiently cured temperatures, and sample age	CS	1347	[88]
19	SVM	PC, GGBFS, FAS, SP, aggregates, water, and sample age	CS	1030	[85]
20	SVM	PC, GGBFS, FAS, SP, water, and sample age	CS	1030	[89]
21	SVM	PC, SP, aggregates, water, and sample age	CS	239	[90]
22	SVM	PC, GGBFS, FAS, SP, aggregates, water, and sample age	CS	1761	[91]
23	SVM	Water/solid ratio, Alkaline activator/binder ratio,Na-Silicate/NaOH ratio, FAS/GGBFS ratio, and NaOH molarity	CS	1030	[82]
24	ET, DT, GEP	PC, FAS, SP, aggregates, water/binder ratio, and sample age	CS	270	[92]
25	ANN, ET, SVM, DT	PC, GGBFS, FAS, SP, aggregates, water, and sample age	CS	1030	[93]
26	SVM	PC, water, FAS, micro-silica, aggregates, flow, HWRR, and VMA	CS	340	[94]
27	SVM	PC, FAS, SP, aggregates, and water	Slump	115	[95]
28	GEP	PC, SP, aggregates, and water	CS	357	[96]
29	RF, GEP	PC, SP, aggregates, and water	CS	357	[97]
30	ANN	PC, CP, FAS, GGBFS, SF, RHA, aggregates, water, SP, and VMA	CS	205	[98]
31	GEP	PC, RHA, aggregates, water, and SP	CS	188	[99]
32	GEP	PC, SF, SP, aggregates, water, and sample age	CS	1030	[100]
33	GEP	PC, BA, aggregates, and water/binder ratio	CS	65	[101]
34	GEP	FAS, NaOH solution, and Na_2SiO_3 gel	CS	210	[102]
35	GEP	FAS, GGBFS, SF, slump flow, T50 cm, L-box, V-funnel, and J-ring; Age	CS, FS, TS	105	[103]
36	ANN, M5P-tree, LR, & MLR	Activated alkaline solution to binder ratio, FAS content, SiO_2/Al_2O_3 of FAS, aggregates content, NaOH and Na_2SiO_3 contents, NaOH/ Na_2SiO_3, molarity, curing temperature, and curing age	CS	510	[72]
37	ANN, M5P-tree, LR, & MLR	Activated alkaline solution to binder ratio, FAS content, SiO_2/Al_2O_3 of FAS, GGBFS content, SiO_2/CaO of GGBFS, aggregates content, NaOH and Na_2SiO_3 contents, NaOH/ Na_2SiO_3, and molarity	CS	220	[71]
38	LR, GA, PSO, SVR, GWO, DE, & MRFO	Water to binder ratio, GGBFS content, aggregates content, water content, curing temperature, and SP	CS	268	[70]
39	ANN, MEP, FQ, LR, & M5P-tree	Alkaline solution to binder ratio, Nano-silica, aggregates, molarity, NaOH content, curing temperature, and concrete age	CS	207	[69]
40	ANN, MEP, FG, LR, MLR, & M5P-tree	Alkaline solution to binder ratio, Nano-silica, aggregates, recycled plastic aggregates, molarity, NaOH content, curing regime, and concrete age	CS	210	[68]

TS and FS denote tensile and flexural strengths, HWRR is high water reducing retarder, SP is superplasticizer, VMA is viscosity-modifying admixture, BA is bagasse ash, CP is calcite powder, and NZ is natural zeolite.

of environmentally friendly concrete [12,13]. This signifies that its manufacture is based on activating aluminosilicate-based source materials with alkali hydroxide/alkali silicate [14]. There is a wealth of literature that demonstrates the use of recycled agricultural and industrial materials as promising geopolymer (aluminosilicate) precursors, including fly ash (FAS), ground granulated blast furnace slag (GGBFS), rice husk ash (RHA), silica fume (SF), red mud (RM), and metakaolin (MK) [15–20]. In contrast to GPC, the prospective application of GGBFS in the production of environmentally and economically viable concrete appears promising, yielding good cost benefit and very less environmental impact [21,22], increased stiffness [23], and high resistance to chemical attacks [24,25] compared to conventional concrete. Corncob ash (CCA) utilization, however, is an emerging development. CCA's high silica content opens up the possibility of employing it in addition to or instead of other pozzolanic materials that are frequently utilized, such as FAS and RHA. On the other hand, aluminosilicate materials are activated using alkaline activators such as sodium hydroxide (NaOH), potassium hydroxide (KOH), sodium silicate (Na_2SiO_3), and potassium silicate (K_2SiO_3) [20,26]. KOH displayed a higher amount of alkalinity than NaOH. However, it has been discovered that NaOH has a better capability for aluminosilicate monomer liberation [27–30]. Research is currently focused on the production of this green concrete at ambiently cured temperature to address the difficulties of site application of oven-cured GPC. It is also crucial to realize that material performance cannot be evaluated merely on the basis of meeting strength standards. Given that all structures are exposed to the elements and frequently endure difficult conditions, durability must be taken into account while estimating their service life. Greater mechanical strengths and improved durability made by GPC make it a suitable concrete option for use in environmentally sensitive areas [31]. Thus, from literature standpoint, GPC has demonstrated favorable and higher mechanical and durability characteristics than PC concrete due to their distinctive chemical makeup [20,26,31]. Ambiently cured GPC exhibited higher compressive strength [32–34], greater flexural strength [35–37], higher tensile

Fig. 1. Aluminosilicate precursor used.

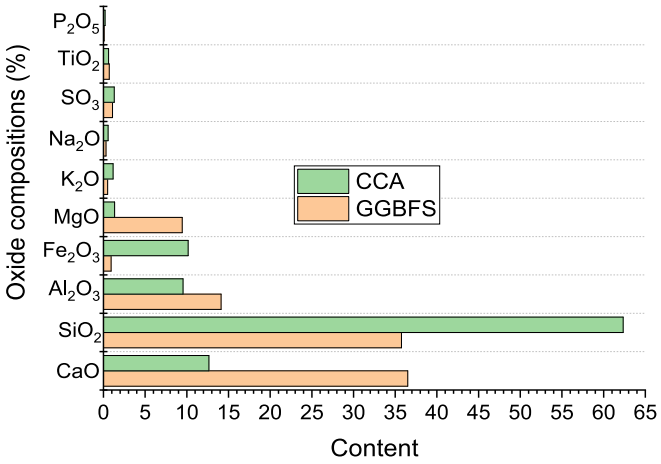

Fig. 2. Oxide compositions of aluminosilicate precursor.

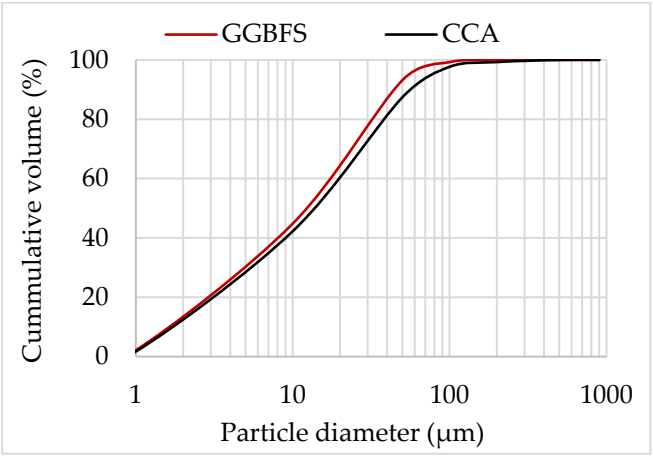

Fig. 3. Particle size distribution of aluminosilicate precursor.

Table 2
Aggregates' properties.

Property	FA	CA
Specific gravity	2.60	2.64
Water absorption (%)	0.32	0.22
Moisture content (%)	0.70	0.80

strength [34,38,39], higher shear strength [40,41], and greater modulus of elasticity [42,43] than PC concrete. In terms of durability traits, GPC has additionally shown higher resistance to acidic attacks [44,45], greater resistance to sulfate attacks [46,47], lower carbonation and permeability [48,49], and lower level of corrosion activity [49,50] than PC concrete. Recently, GPC has been modified with Nano-silica and recycled plastic aggregates and the performance was promising [51–53].

The way engineers, scientists, researchers, and programmers create

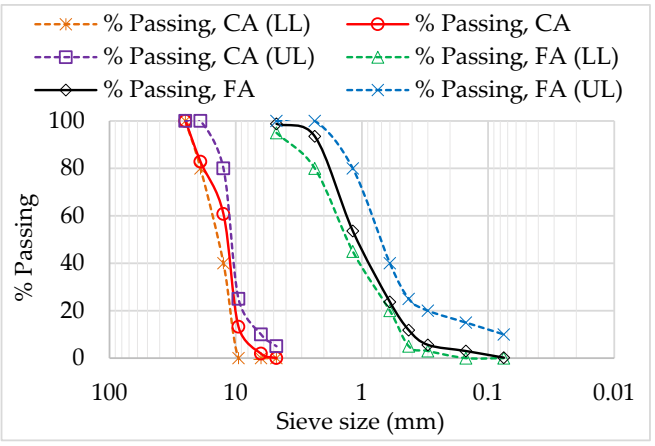

Fig. 4. Aggregates' size distribution.

and enhance products and services is drastically changing as a result of artificial intelligence (AI). Today, AI is used in some capacity across all engineering disciplines, and many industrial difficulties require researchers who are capable of integrating AI into their daily work. However, there were a number of drawbacks and performance issues with AI-based systems. They found it difficult to carry out activities that would normally come naturally to a normal person, such identifying objects or comprehending conversation [54]. Because of this, current AI systems have had difficulty developing substitute techniques for imparting intuition to computers. The aforementioned issues were addressed by incorporating machine learning (ML) into AI systems [54,55]. Machine learning algorithms enable machines to acquire the information they need to do a specific task by studying a sufficient number of data samples [56,57]. The properties that best characterize the most particular data must be retrieved before the method can be used. This procedure is known as feature extraction. The sample data utilized in the subsequent stage of the procedure, which instructs the system to transmit features and separate patterns using machine learning, is based on a particular training strategy [54,58,59]. Today's research focuses on using statistical methods and AI to handle more complicated challenges in civil engineering. These AI and statistical techniques are mostly used in civil engineering to forecast the concrete compressive strength (CS) [17,60]. A few researchers have also used them to solve more challenging issues, including the strength and slump prediction in self-compacting concrete [61], the prediction of the axial behavior of various columns [62], the prediction of the shear behavior of beams [63], the prediction of chloride penetration [64], and others. The importance of these forecasts resides in the fact that it decreases the number of trial mixtures required for more study, reducing the cost and duration of studies. The most popular ML methods for predicting concrete strength are artificial neural networks (ANN), decision tree (DT), ensemble of tree (ET), Gaussian process regression (GPR), gene expression programming (GEP), random tree (RT), support vector machine (SVM), and others [65–67]. In addition to these, linear regression (LR), multi-logistic regression (MLR), full quadratic (FG), M5P-tree, genetic algorithms (GA), grey wolf optimization (GWO), particle swarm optimization (PSO), differential evolution (DE), multi-expression programming (MEP), and mantra rays foraging optimization (MRFO) have been recently engaged in the prediction of compressive strength of GPC [68–72]. The ANN model demonstrated more precision in the prediction of the compressive strength of GPC than the other models. Table 1 provides information on several ML techniques used to forecast concrete properties.

To address the issues with manually created traits in sophisticated AI programs, deep learning techniques were developed [54,58]. Advances in neuroscience serve as inspiration for deep learning, which is congruent with how the nervous system interprets information and

Table 3
Mix design proportions.

Grade	Mix ID	kg/m^3 GGBFS	CCA	kg/m^3 FA	CA	12 M (kg/m^3) Water	SHP	14 M (kg/m^3) Water	SHP	16 M (kg/m^3) Water	SHP	kg/m^3 SSG
	GC0	380	0	899	1045	37.86	20.74	35.16	23.44	32.64	25.96	146.4
M 30	GC20	304	76	887	1045	37.86	20.74	35.16	23.44	32.64	25.96	146.4
MPa	GC40	228	152	874	1045	37.86	20.74	35.16	23.44	32.64	25.96	146.4
	GC60	152	228	865	1045	37.86	20.74	35.16	23.44	32.64	25.96	146.4
	GC80	76	304	852	1045	37.86	20.74	35.16	23.44	32.64	25.96	146.4
	GC100	0	380	841	1045	37.86	20.74	35.16	23.44	32.64	25.96	146.4
	GA0	488	0	805	1045	37.86	20.74	35.16	23.44	32.64	25.96	146.4
M 40	GA20	390	98	788	1045	37.86	20.74	35.16	23.44	32.64	25.96	146.4
	GA40	293	195	772	1045	37.86	20.74	35.16	23.44	32.64	25.96	146.4
MPa	GA60	195	293	758	1045	37.86	20.74	35.16	23.44	32.64	25.96	146.4
	GA80	98	390	741	1045	37.86	20.74	35.16	23.44	32.64	25.96	146.4
	GA100	0	488	728	1045	37.86	20.74	35.16	23.44	32.64	25.96	146.4

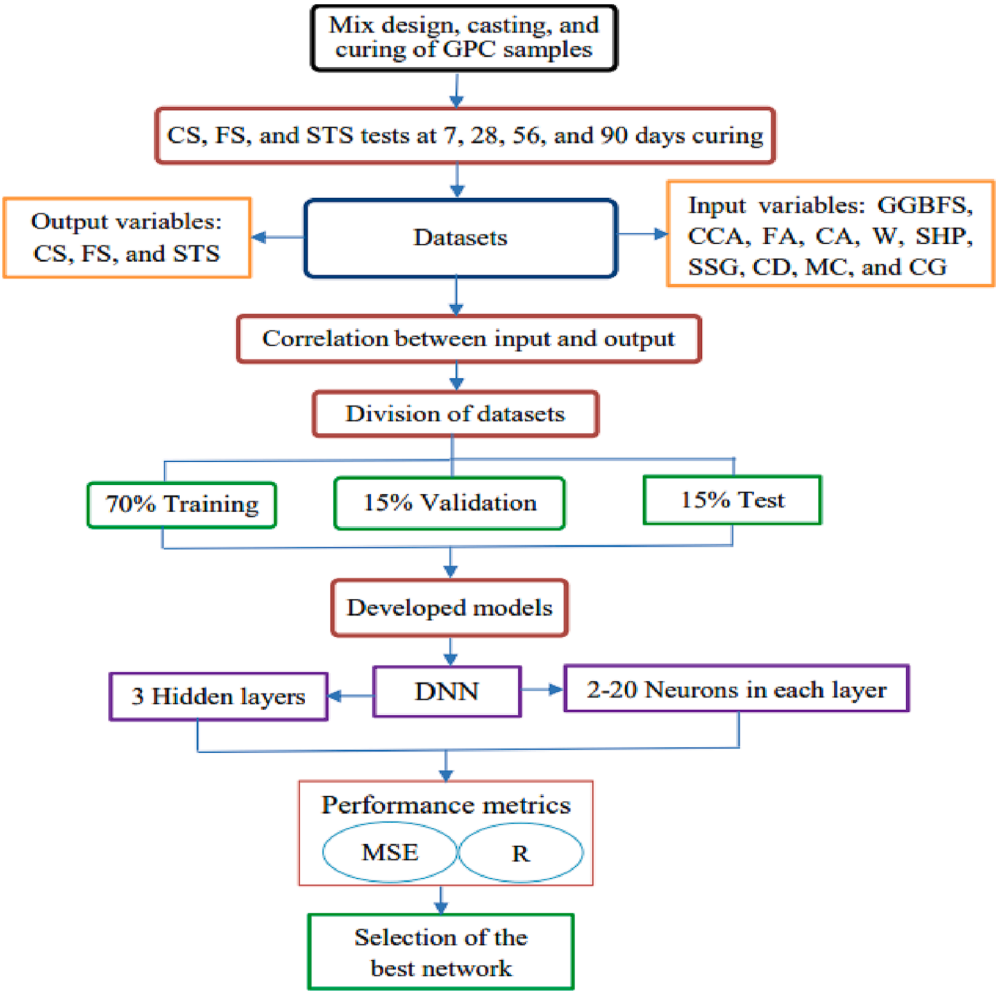

Fig. 5. Graphical representation of the flowchart engaged in this study.

communicates. The hidden layers of an ANN and a number of intricate formulae are layers utilized in deep learning [73]. As a result, deep learning algorithms supports both feature extraction and correlations between features and intended output [54,73–75].

There is a gap from earlier studies illustrated in Table 1 due to meagre research into aluminosilicate binders used (GGBFS and CCA), concrete mix grades (M 30 and M 40), and concentrations of sodium hydroxide solutions (12, 14, and 16 M). Besides, previous studies showed a little or no application of deep neural network (DNN) of the AI technique in the prediction of GPC strengths. These are the motivations behind this study's conduct. In general, concrete testing processes take a long time, and mistakes during experiments are inevitable. After the concrete has been cast and cured for 28 days, a normal compression test is conducted. If the test findings are below the acceptable strength, expensive remediation measures are unavoidable. As a result, it is crucial to forecast concrete's strength before using it on construction sites. Using deep learning techniques, it is now possible to classify and generalize existing experimental results to forecast concrete strengths based on the mix's constituents. Consequently, the effects of 10 parameters, including the contents of ground granulated blast furnace slag (GGBSF), corncob ash (CCA), fine aggregates (FA), coarse aggregates (CA), water (W), sodium hydroxide pellets (SHP), sodium silicate gel

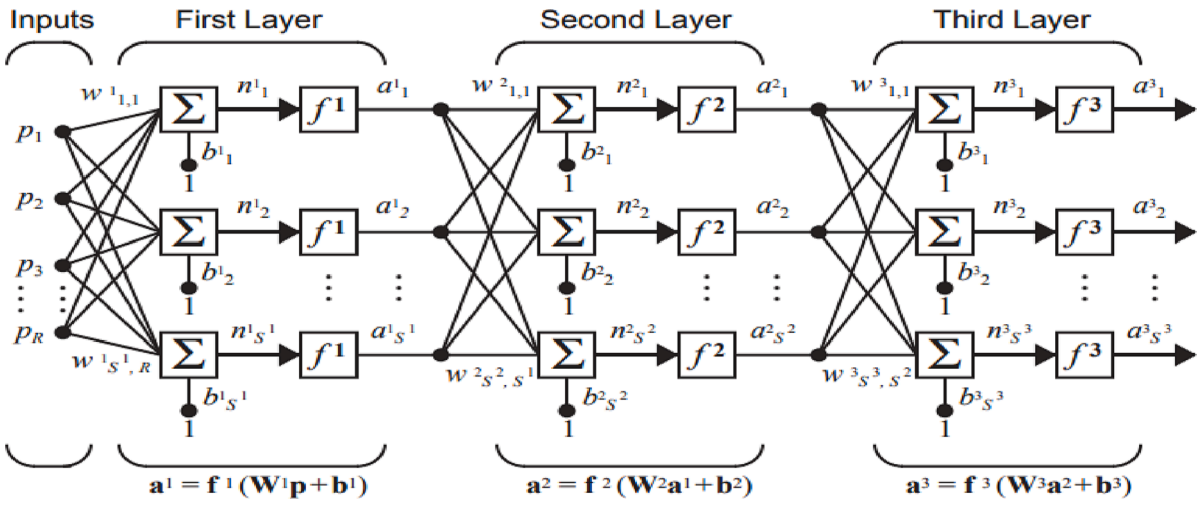

Fig. 6. A-3 hidden layer network [116].

(SSG), curing days, molarity concentrations (MC) of sodium hydroxide solution, and concrete grades were examined and evaluated on the compressive strength, flexural strength, and split tensile strength of GGBSFA-GPC. Deep neural network techniques of 3 hidden layers and 2–10 neurons in each hidden layer were engaged. The experimental test results under ambiently cured circumstances were employed as prediction models to forecast the compressive strength, flexural strength, and split tensile strength of GGBSF-CCA-GPC at 7, 28, 56, and 90 days. To achieve this, 288 experimental samples of cubes, beams, and cylinders were experimentally cast and processed for compressive, flexural, and split tensile strengths, respectively. Of these samples, 260 were utilized as training datasets, while the remaining 28 were used as untrained datasets to validate the new proposed model. After that, deep learning models were built using a variety of network topologies to forecast the concrete strengths. The predicted strengths were compared with experimental strengths.

The research's relevance is that it guarantees the usage of the developed models in the construction and building sector without any theoretical analysis. It performs statistical analysis and evaluates the effects of various parameters on the compressive strength, flexural strength, and split tensile strength of GGBSF-CCA-GPC. With composite blends comprising a wide variety of factors, the research quantifies and offers a deep neural network model to forecast the compressive strength, flexural strength, and split tensile strength of GGBSF-CCA-GPC. It aids in identifying the ideal network topology for GGBSF-CCA- GPC's compressive strength, flexural strength, and split tensile strength prediction from numerous hidden layers and neurons. Besides, conserving resources, time, and cost is made possible by the development of DNN tools and their use in the construction and building sector, particularly for forecasting the mechanical properties of geopolymer concrete. Finally, the utilization of recycled agro-industrial waste materials as full or partial replacement of cement in concrete production improves concrete's properties and eases pressure on natural resources.

2. Materials and methods

2.1. Materials

All materials used, aluminosilicate precursor (slag and corncobs), aggregates, water, and alkaline activating precursor (NaOH pellets [SHP] and Na_2SiO_3 gel [SSG]), were sourced locally. The blast furnace slag was processed by pulverizing it with Los Angeles Abrasion machine (Model: UTC-0600-T), producing GGBFS. Corncobs were processed in a closed combustion with a gas furnace at 600 °C for 2 h, yielding approximately 30 wt% CCA. To produce finer particle size, both CCA and GGBFS, as shown in Fig. 1, were then sieved with a 45-μm size. The aluminosilicate precursor's physical properties, specific gravity and surface area, were determined in line with the BS EN standard [104], while their fineness was evaluated in consonant with BS EN code [105]. The results revealed 3.10 and 2.64 as specific gravity; 425 m^2/kg and 515 m^2/kg as specific surface area; and 7.60% and 8.10% as fineness for GGBFS and CCA, respectively. Fig. 2 presents the results of chemical compositions analyzed with the aid of XRF spectrophotometer machine, Philips PW-1800 at 800 °C loss of ignition. Fig. 3 displays the particle size distribution of the aluminosilicate precursor as measured by the Laser diffraction, Model Beckman Coulter LS-100. The SG of CCA is lower than GGBFS. However, CCA showed higher fineness and SSA than GGBFS, indicating that additional CCA and water would be needed when GGBFS is partially replaced with CCA [106].

Granites with a particle size range of 12.5 to 19 mm and sharp sand with a particle size range of 0 to 4.5 mm were used as fine aggregates (FA) and coarse aggregates (CA), respectively. Table 2 provides the aggregates' physical test results, and Fig. 4 displays the aggregates' grade, including lower limits (LL) and upper limits (UL), as determined by the BS EN standard [107].

2.2. Mix design, preparation, and curing

Contrary to Portland cement concrete, GPC requires a different mix design, and there is no any established standards for it yet. ACI 211-1 [108]'s procedure was modified and used for the mix design proportions as well as recommendations from literature [19,26,72,109]. In the course of mix design, specific gravity of all constituents, fineness moduli of fine aggregates, water absorption and moisture content of fine and coarse aggregates were put into consideration. The mixtures, known as GC0 and GA0, were cast for GPC sample made entirely of GGBFS as a control composite for grades 30 MPa and 40 MPa concrete, respectively. A replacement percent of 20–100 wt% of CCA was used to prepare subsequent mixes in place of GGBFS. The geopolymer mixtures were proportioned using different concentrations of NaOH (12 M, 14 M, and 16 M), with a widely used 2.5 mass ratio of Na_2SiO_3 to NaOH solution [1,38,110,111]. The NaOH utilized was 99% pure, commercial grade, and in pellet form. As a result, 354 g, 400 g, and 443 g of SHP were mixed with 646 g, 600 g, and 557 g of water to produce 1 L solution [112], and then SSG was added to the mixture to get the desired concentration. For the attainment of exothermal heat solution at room temperature, the activating precursor was made 24 h prior to the casting of concrete [1,38]. To prevent NaOH from building up at the bottom of the container, the prepared solution was stirred thoroughly for 5 min. Thereafter, aluminosilicate precursor and aggregates were mixed for 3

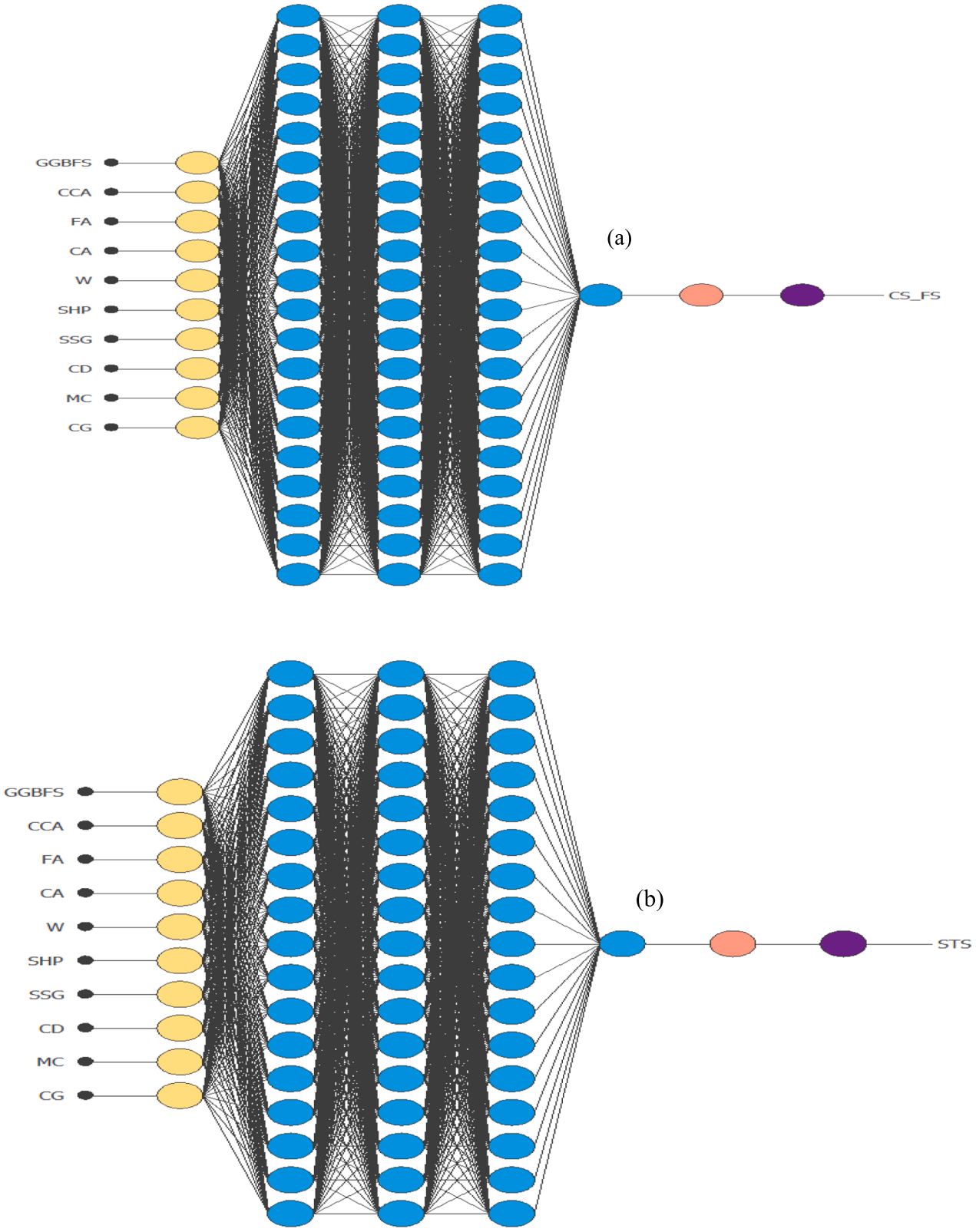

Fig. 7. The best deep neural network structures for predicting (a) compressive and flexural strengths (10–20–20–20-1) and (b) split tensile strength (10–17–17–17-1).

Table 4
Statistical parameters of slag-ash-based GPC used in the training datasets.

Parameter	Unit	Minimum	Maximum	Median	Mean	SD	Variable
GGBFS	kg/m^3	0	488	228	218.65	153.61	Input
CCA	kg/m^3	0	488	195	215.24	152.49	Input
FA	kg/m^3	728	899	841	818.12	56.79	Input
CA	kg/m^3	1045	1045	1045	1045	0	Input
W	kg/m^3	32.65	37.86	35.16	35.22	2.15	Input
SHP	kg/m^3	20.74	25.96	23.44	23.38	2.15	Input
SSG	kg/m^3	146.40	146.40	146.40	146.40	0	Input
CD	Day	7	90	42	45.25	31.14	Input
MC	M	12	16	14	14	1.65	Input
CG	MPa	30	40	30	34.96	5	Input
CS	MPa	10.67	64.09	36.05	35.90	12.17	Output
FS	MPa	2.81	7.45	5.47	5.36	1.01	Output
STS	MPa	1.97	6.54	3.60	3.65	0.66	Output

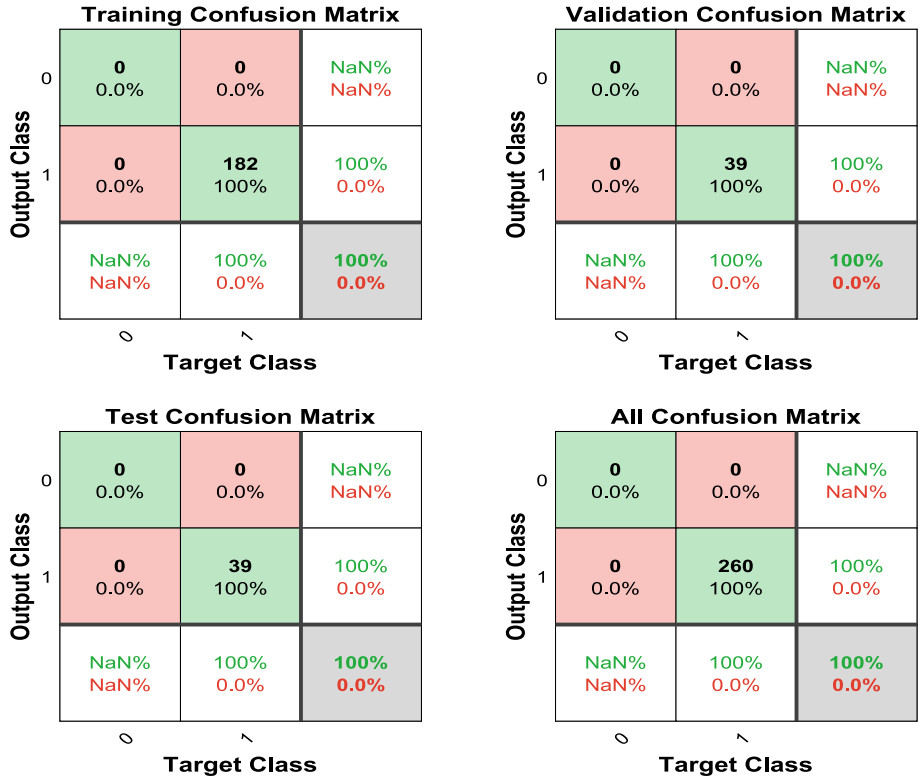

Fig. 8. Confusion matrix plots.

min before activating precursor was added. This wet mixture was further mixed for 5 min to obtain uniform blend. Following that, the mixture was formed into cubes, prismatic beams, and cylinders in accordance with the applicable standards for determining compressive strength [113], flexural strength [114], and split tensile strength [115], respectively. After 72 h, the samples were demolded, and they were all ambiently cured for 7 to 90 days at 23 ± 5 °C and 65 ± 5 RH. Table 3 shows the mix design proportions of the concrete produced.

2.3. Experimental tests

The 150 mm^3 concrete cube samples were crushed using a motorized COMTEST 3000 kN automated compression machine by applying the load gradually at 3 kN/s for the compressive strength test. The peak load applied when the failure occurred was recorded and the compressive strength was determined.

Flexural strength was evaluated using a prismatic beam samples of 500 mm × 100 mm × 100 mm size. For this test, prismatic samples were placed on an automated flexural testing equipment, which applied a three-point bending load on them.

Cylindrical molds with a 100 mm diameter and 200 mm height were used for the split tensile strength tests. The specimens were positioned horizontally, a rate of 1.2 N/(mm^2/min) to 2.4 N/(mm^2/min) was used for continuous loading, and the failure load was taken. Two samples were cast for each mix proportion, and they were evaluated at ages 7, 28, 56, and 90 days. Figure 5 provides a flowchart, which describes the steps for the work process.

2.4. Artificial intelligence

2.4.1. Deep neural networks (DNN) and datasets

It is timely and costly to investigate concrete strength through laboratory testing. It is challenging to determine strength accurately since various elements, like geopolymer, influence it. To accomplish this, we therefore need a numerical model, or soft computing methods. Consequently, deep neural network has become extremely popular in scientific computing, and businesses that deal with complicated issues frequently employ its techniques. In this study, a deep neural network

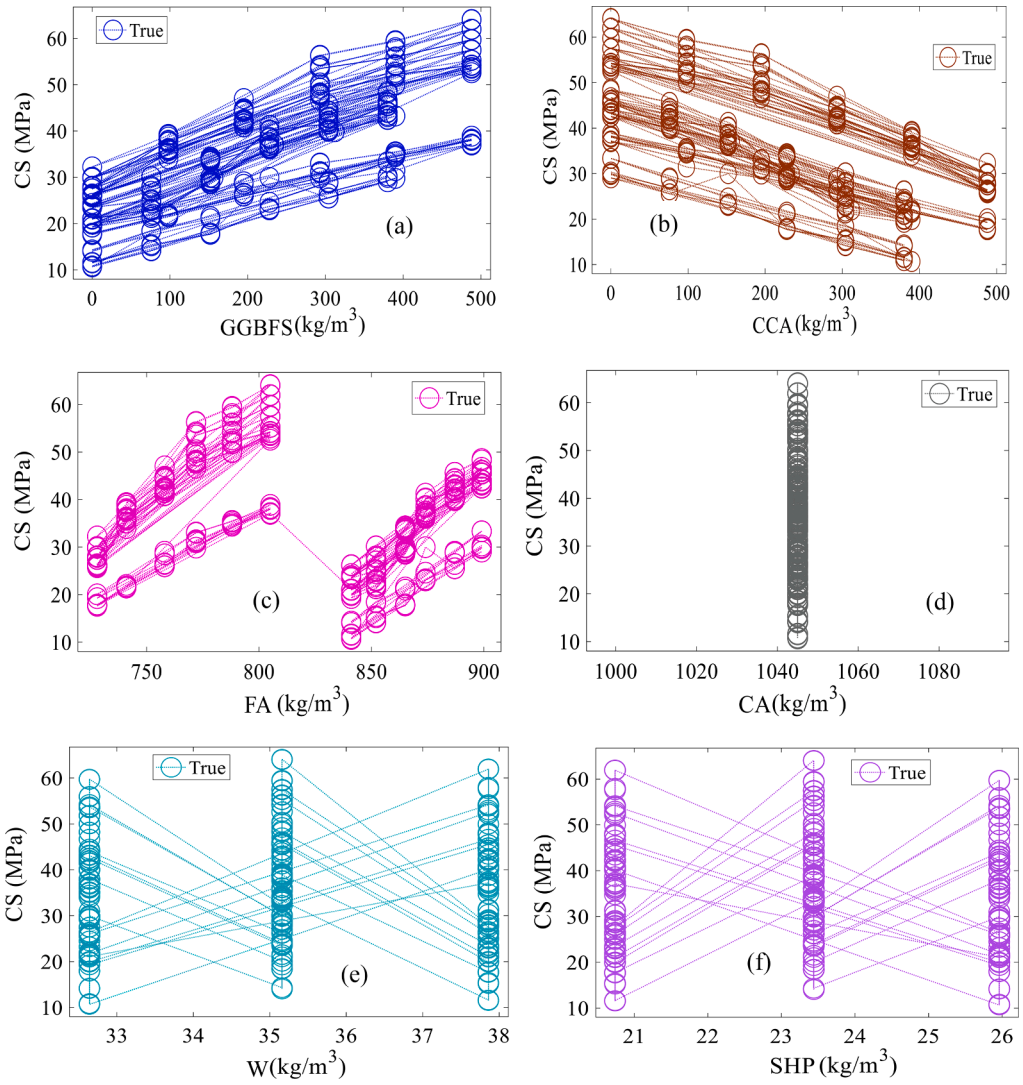

Fig. 9. Response plots between the target (compressive strength) and (a) GGBFS, (b) CCA, (c) FA, (d) CA, (e) W, (f) SHP, (g) SSG, (h) CD, (i) MC, and (j) CG.

model was created in order to increase prediction accuracy with a bigger dataset sample size and the flexibility of employing multiple combinations of input variables. The specimen geometry, GGBFS, CCA, FA, CA, water (W), SHP, SSG, molar concentration (MC), curing day (CD), and concrete grade (CG) are the 10 input parameters used to develop a DNN model to achieve this objective. The problem's targets were the GPC's produced compressive strength (CS), flexural strength (FS), and split tensile strength (STS). A 288 datasets altogether was obtained from the experimental results for each strength. Of the 260 datasets utilized for learning, 70%, 15%, and 15% were used for training, validation, and testing, respectively. The remaining 28 datasets were used as untrained datasets for validating the developed deep neural network model. The multilayer perceptron, train by the backpropagation algorithm, is currently the most popular neural network [116], hence the Levenberg-Marquardt of backpropagation training algorithm was used to train the developed deep neural network. Compared to single-layer networks, multilayer networks are more powerful. For example, it is possible to train a two-layer network with a sigmoid first layer and a linear second layer to mimic the majority of functions arbitrarily well. This is not possible with single layer networks [116]. Most realistic neural networks only contain two or three layers, on average. Rarely are four or more layers employed [116–118]. On this basis, a 3-hidden layer with 2–20 neurons in each layer was engaged to investigate the influence of varying neurons in deep neural network architecture. However, because of the additional abstraction classes, which enable them to train datasets in a way that is rare-dependent, the deep neural network model is vulnerable to overfitting [119]. As a result, a function was fitted and set with a random stream in this study to prevent overfitting. Fig. 6 cascades a typical deep neural network with 3-hidden layer network. According to Fig. 5, the third network receives the second network's output as its input, and the first network's output serves as the input for the second network. The number of neurons in each layer and even the transfer function might vary. The output of the third network is thus shown in Eq. (1):

$$a^3 = f^3\left(W^3 f^2\left(W^2 f^1\left(W^1 p + b^1\right) + b^2 + b^3\right)\right) \tag{1}$$

In multilayer networks, one layer's output serves as the next layer's input. Eq. (2) provides an illustration of this operation.

$$a^{m+1} = f^{m+1}\left(W^{m+1} a^m + b^{m+1}\right) for\, m = 0, 1, \cdots, M-1 \tag{2}$$

where M represents the network's layer number.

According to Eq. (4), the first layer's neurons get inputs from external sources. This gives Eq. (3) its starting point.

$$a^0 = p \tag{3}$$

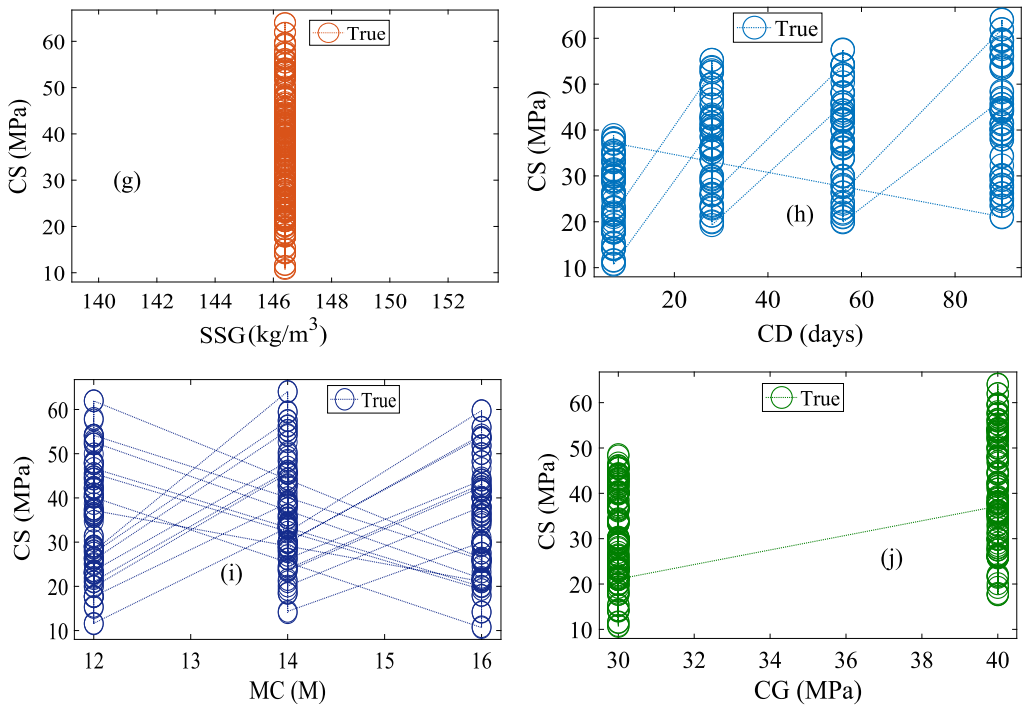

Fig. 9. (*continued*).

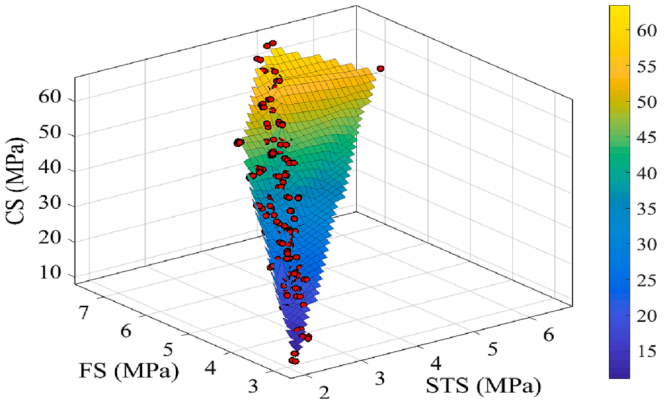

Fig. 10. The connection amongst compressive, flexural, and split tensile strengths.

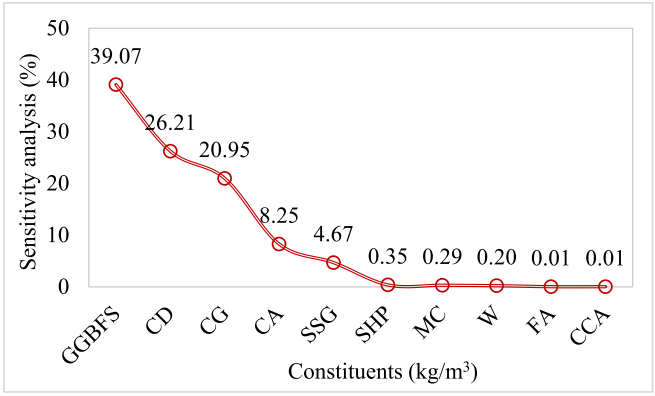

Fig. 11. Sensitivity analysis for the CS of GGBFS-CCA- based GPC.

The final layer's neurons' outputs, as given in Eq. (4), are referred to as the network outputs:

$$a = a^M \tag{4}$$

2.4.2. Performance index

The Levenberg-Marquardt algorithm is a generalization of the backpropagation algorithm for multilayer networks, and both techniques employ the same performance metric, mean square error (MSE). A set of appropriate network behavior examples are given to the algorithm in Eq. (5):

$$\{p_1, t_1\}, \{p_2, t_2\}, \cdots, \{p_q, t_q\}, \tag{5}$$

where p_q is a network input and t_q is the intended target output.

The network output is compared to the target as each input is applied to the network. According to Eq. (6), the algorithm should modify the network settings to reduce mean square error:

$$F(x) = E\left[e^2\right] = E\left[(t-a)^2\right] \tag{6}$$

where x represents the weights and biases vector for the network.

In the event that the network has several outputs, this generalizes to the relationship shown in Eq. (7), while Eq. (8) represents the MSE approximation based on the Levenberg-Marquardt technique, where the squared error at iteration k has taken the place of the expected squared error.

$$F(x) = E\left[e^T e\right] = E\left[(t-a)^T (t-a)\right] \tag{7}$$

$$F(x) = (t(k) - a(k))^T (t(k) - a(k)) = e^T(e)e(k) \tag{8}$$

Ultimately, MSE and R (correlation coefficient) demonstrated the DNN models' efficiency to forecast with accuracy. Mathematically, DNN models are more accurate when the R-value is close to 1 and the MSE value is close to 0. These performance metrics are illustrated in Eqs. (9) and (10). Fig. 7 displays the best DNN architecture in terms of performance metrics, with 10 inputs, 3 hidden layers, each with 10 neurons, and one output (10–10–10–10-1).

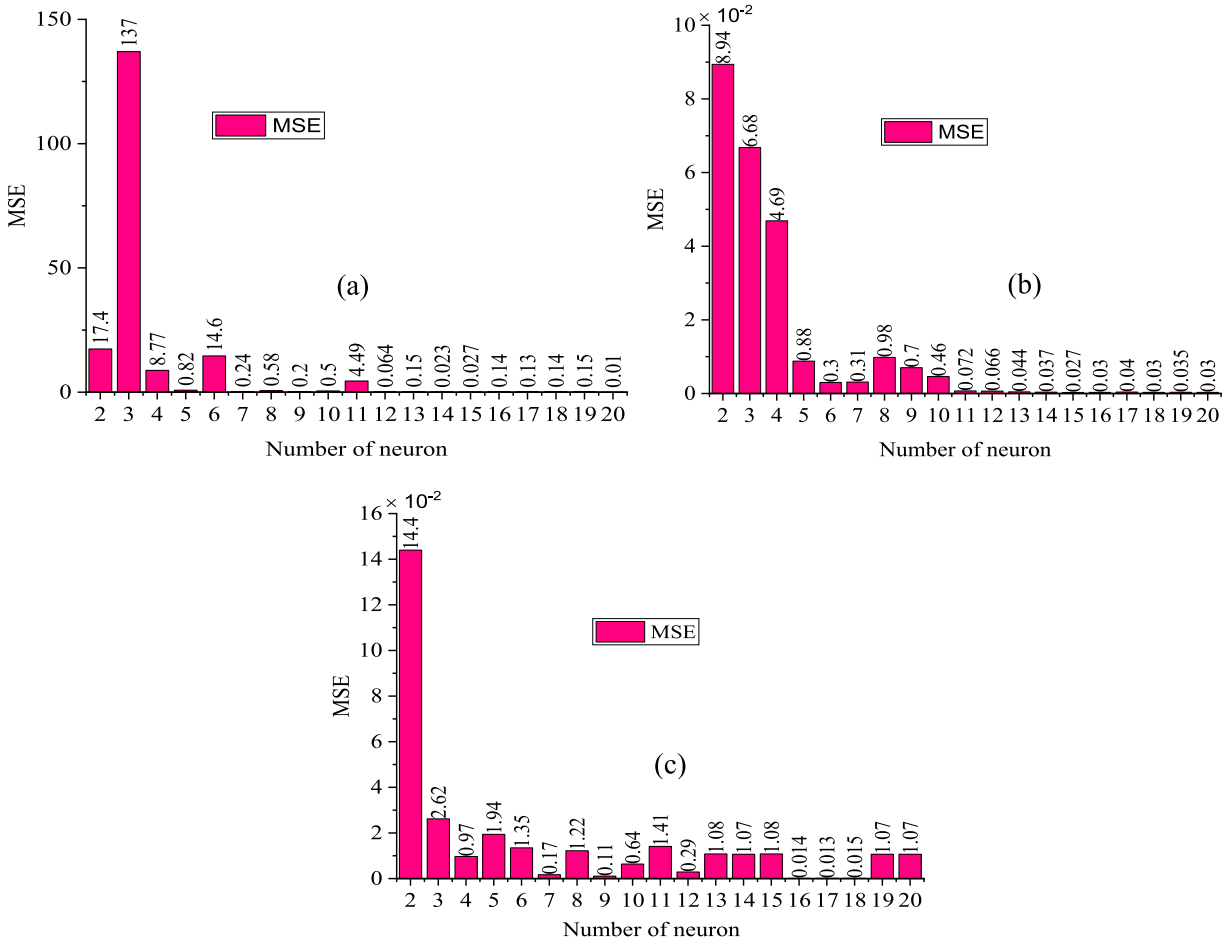

Fig. 12. MSE outputs for (a) compressive strength, (b) flexural strength, and (c) split tensile strength.

$$MSE = \frac{1}{n}\sum_{i=1}^{n}\left(y_i^{pred} - y_i^{true}\right)^2 \tag{9}$$

$$R = 1 - \frac{\sum_{i=1}^{n}\left(y_i^{pred} - y_i^{true}\right)}{\sum_{i=1}^{n}\left(y_i^{pred} - \overline{y_i^{true}}\right)} \tag{10}$$

3. Results and discussion

3.1. Statistical datasets

In order to run the deep neural networks, a total of 260 pairs of input/target values were constructed using different GPC mix design proportions. The statistical analysis the experimental datasets are summarized in Table 4. The statistical findings in Table 4 provide succinct and clear values to illustrate trends or patterns in the predictive analysis. This affirms the matrix displayed in Fig. 8.

Using Fig. 7, 182 samples are correctly recognized as the training matrix. This is the same as 70% of all samples. In sum, all of the forecasts are 100% true. In addition, 39 samples, or 15% of all samples, are also designated as test matrices and validation matrices, respectively. Overall, every prediction was exact (100%). Finally, 260 samples are identified as being part of the full-trained matrix, and all predictions are 100% accurate.

3.2. Concrete mix constituents responses

The anticipated response is shown in Fig. 9 in comparison to the input arguments to show the relationship between the various predictors and the response (compressive strength), which is also comparable to flexural strength and split tensile strength. The majority of predictors were seen in Fig. 9 to have an impact on the strength performance. These results, in accordance with pertinent studies, demonstrate that the aluminosilicate precursor's chemical and mineralogical compositions, the ratio of an alkaline activating precursor to a binder, the concentration of a sodium hydroxide solution, the ratio of a sodium silicate to sodium hydroxide solution, the amount of extra water present, the curing temperature, and the specimen age are the variables that have the greatest direct influence on the compressive strength of GPC [120,121].

When finely ground, GGBFS exhibits outstanding characteristics and can replace 35–70% of the OPC content. It is then mixed with other precursor to manufacture GPC [122]. The mono-silicates of Q^o-type found in the glass particles of GGBFS, along with its amorphous nature with irregularly shaped particles and the relatively wider hump, are the same ones found in OPC clinker and dissolve in any media once initiated, generating higher reactivity compared with pozzolan (CCA in this case) and enhancing the mechanical properties of GPC [123,124]. Considering all of these advantages reveals the rationale behind why GGBFS enhances strength in Fig. 9(a) whereas CCA decreases strength in Fig. 9 (b) with increasing content in GPC mixture. The easy availability of free Ca^{2+} ions, which react with alumina and silica to produce calcium-aluminate-silica-hydrate (C-A-S-H) gel and with geopolymer gels causes alkaline activating precursor series to increase as GGBFS content rises, resulting in an increase in compressive strength [125,126]. In addition, the reaction between the alkaline activating precursor and GGBFS is exothermic, producing heat that aids in the geopolymerization process. As a result, the compressive strength of GPC rose as the content of GGBFS increased [127]. Due to this, findings from experimental tests showed that 60% GGBFS and 40% CCA provided the best compressive

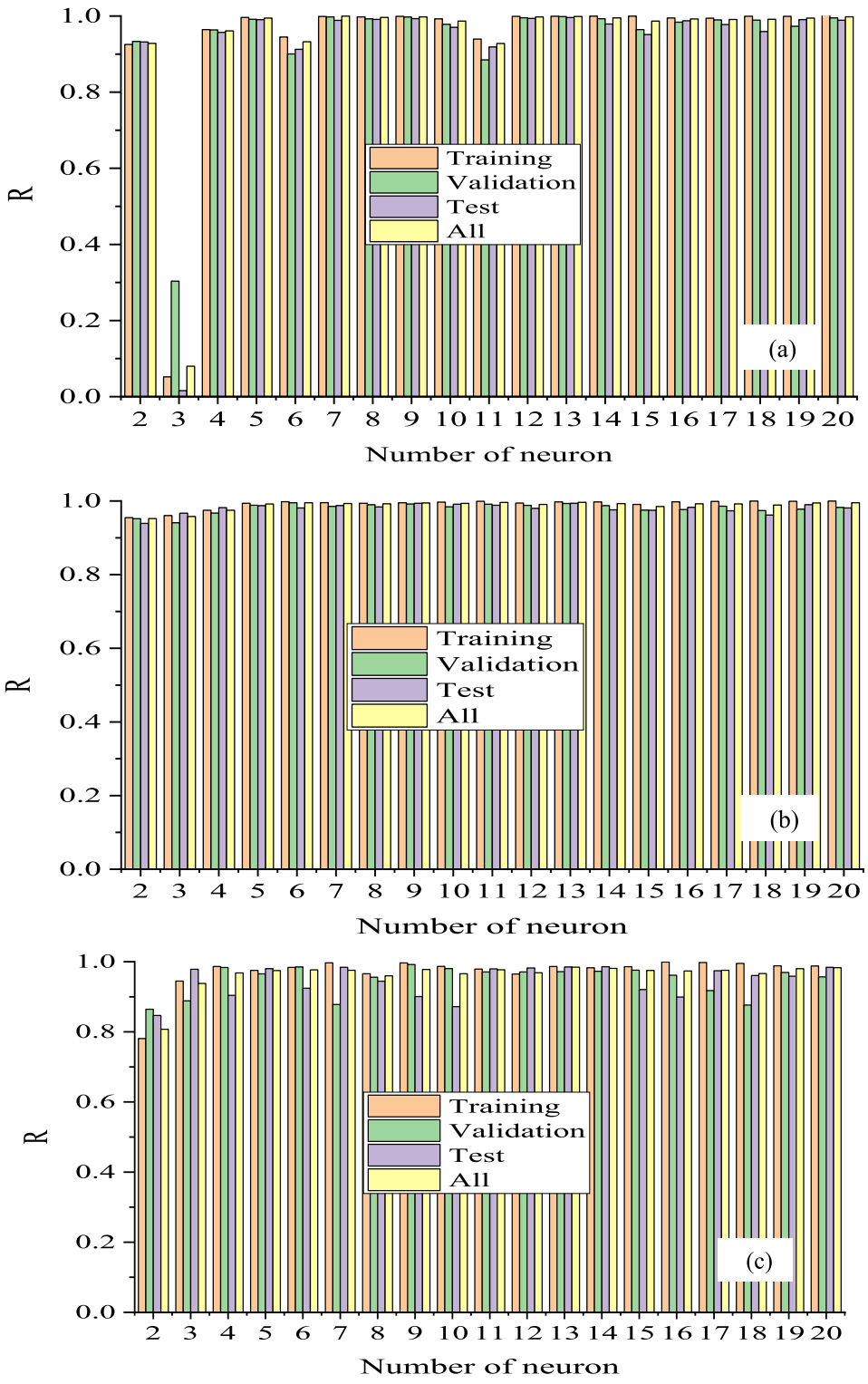

Fig. 13. Coefficient of correlation (R) outputs for (a) compressive strength, (b) flexural strength, and (c) split tensile strength.

strength (64.09 MPa). This is in line with relevant study, which found that 70% GGBFS and 30% fly ash mix proportion provided the best compressive strength of 66 MPa [128].

From Figs. 9(c) and (d), it was clear that the strength improved with increasing aluminosilicate precursor to aggregates ratio due to the packing capability between the constituents. The aggregated proportions in this investigation are consistent with prior research, where the best compressive strength of GPC was attained at 70% optimal coarse aggregates and the maximum fine aggregates to coarse aggregates ratio was 35% [129]. The components of coarse and fine aggregates, according to pertinent studies, did not appear to have a sizable impact on strength because the shape, particle size distribution, and interface transition zone (ITZ) of aggregates had a greater impact on strength growth than their contents [17,130,131]. Additionally, it is clear from Fig. 9(h) that the strength grew as the number of curing days rose from 7 to 90 days.

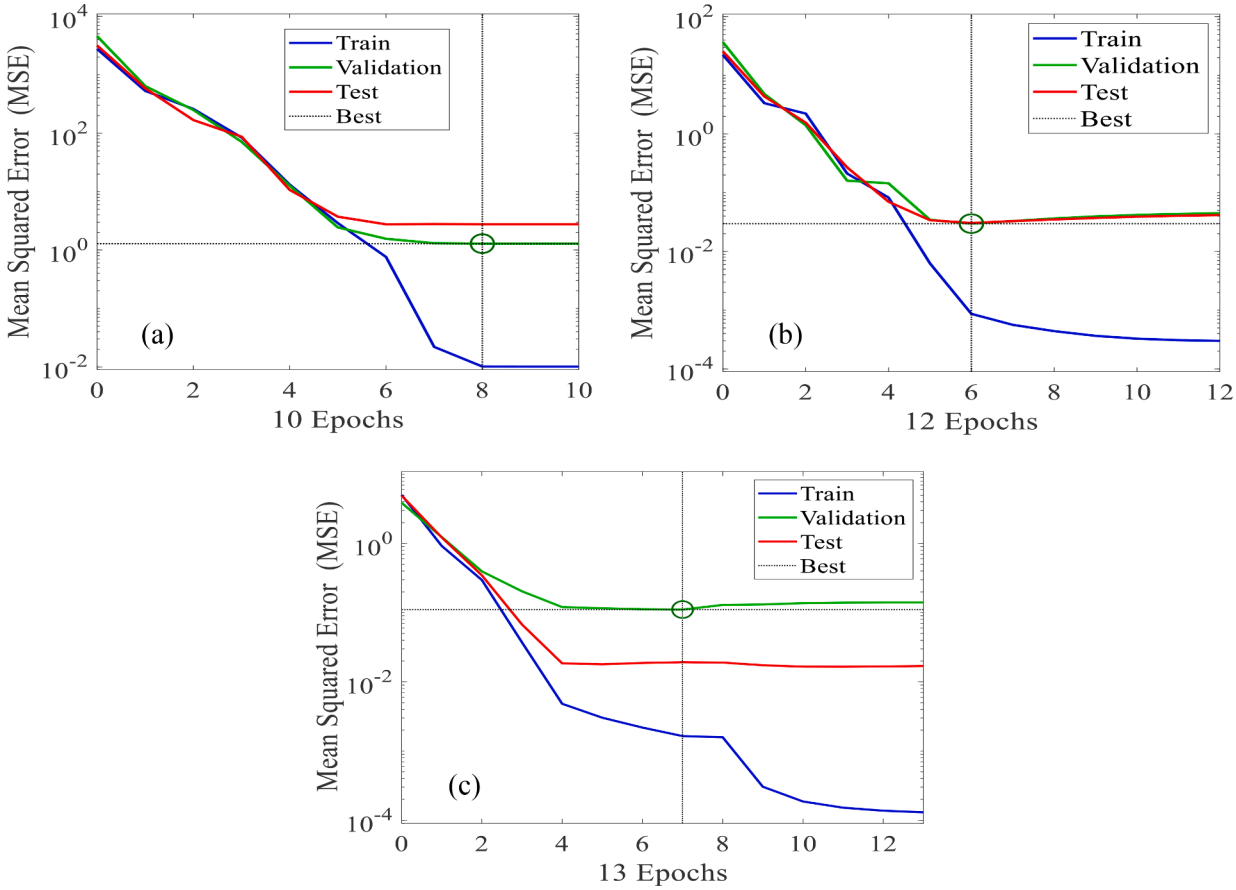

Fig. 14. Best performance validation for (a) compressive strength, (b) flexural strength, and (c) split tensile strength.

Researchers have also extensively examined the molarity of sodium hydroxide solution as a subject that influences the performance of GPC. When compared to normal concrete, GPC's compressive strength increases as the molarity of sodium hydroxide solution increases [132,133]. This could be because Si and Al particles completely disintegrate during the polymerization process; Al and Si particles dissolve faster when the sodium hydroxide molarity is higher. This results in stronger GPC mixes with more sodium hydroxide solution [120]. Regarding the 14 M shown to be the top performing activator in this investigation (see Fig. 9(i)), earlier studies also found that 14 M supplied the highest compressive strength to GPC [42,124,126,127,134]. As a result, increasing the molar concentration of the sodium hydroxide solution generally increased the compressive strength, especially when it exceeded 12 M [17]. A few research, however, asserted that the 10 M [129], 12 M [135], and 16 M [136] of sodium hydroxide yielded GPC with the highest compressive strength. Additionally, different studies indicated that the 2.5 ratio of sodium silicate gel to sodium hydroxide solution, which was chosen for this investigation, performed better than the 1 and 3 ratios [129,136].

According to Fig. 9(j), the rise in compressive strength of GPC for M 40 compared to M 30 with alkaline activating agent to aluminosilicate precursor was due to the reduction in alkaline activating agent to aluminosilicate precursor from 0.54 to 0.42. This supports earlier research that found that increasing the alkaline liquid to binder ratio decreased the compressive strength of GPC [137]. However, relevant results showed that the compressive strength of GPC rose with a rise in the alkaline solution/binder ratio up to 0.40 before being reversed [136]. In a similar vein, the compressive strength of GPC was increased to an alkaline solution to binder ratio of 0.55 [129].

The piecewise linear association between compressive, flexural, and split tensile strengths is depicted in Fig. 10. It is clear from Fig. 10 that as the compressive strength rises, the flexural and split tensile strengths rise as well. As a result, the flexural and split tensile strengths were also impacted by the variable parameters that were mentioned above that affect the performance of the compressive strength of GPC. Ultimately, according to relevant research, the ratio between fine and coarse aggregates, as well as between sodium silicate and sodium hydroxide solutions, should be thoroughly assessed before the GPC production process to prevent adverse effects on strength growth [138].

3.3. *Sensitivity analysis*

Sensitivity analysis approach was used to quantify the impact of input factors on the output parameter (compressive strength). This technique identifies the input parameters that the output parameter in the desired network is most sensitive to, in order to specify the index that will have the greatest impact on the network's output. Fig. 11 shows the findings of the output sensitivity analysis of the model in relation to the input parameters. In relation to Fig. 11, GGBFS and CCA parameters yielded, respectively, the greatest and the least impact on the compressive strength of the deep neural network model. The findings are in line relevant studies, where fly ash yielded about 28% [60] and 36% [138] sensitivity indexes in the production of GPC. Moreover, Ahmed et al. [71] applied soft computing models to forecast the compressive strength of GGBFS-fly ash-based geopolymer concrete. The sensitivity analysis signified that the contents of fly ash, GGBFS, sodium silicate, and sodium hydroxide are the most influencing variables for predicting the compressive strength of the GGBFS-fly ash GPC with 0.209, 0.203, 0.204, and 0.204 magnitudes, respectively.

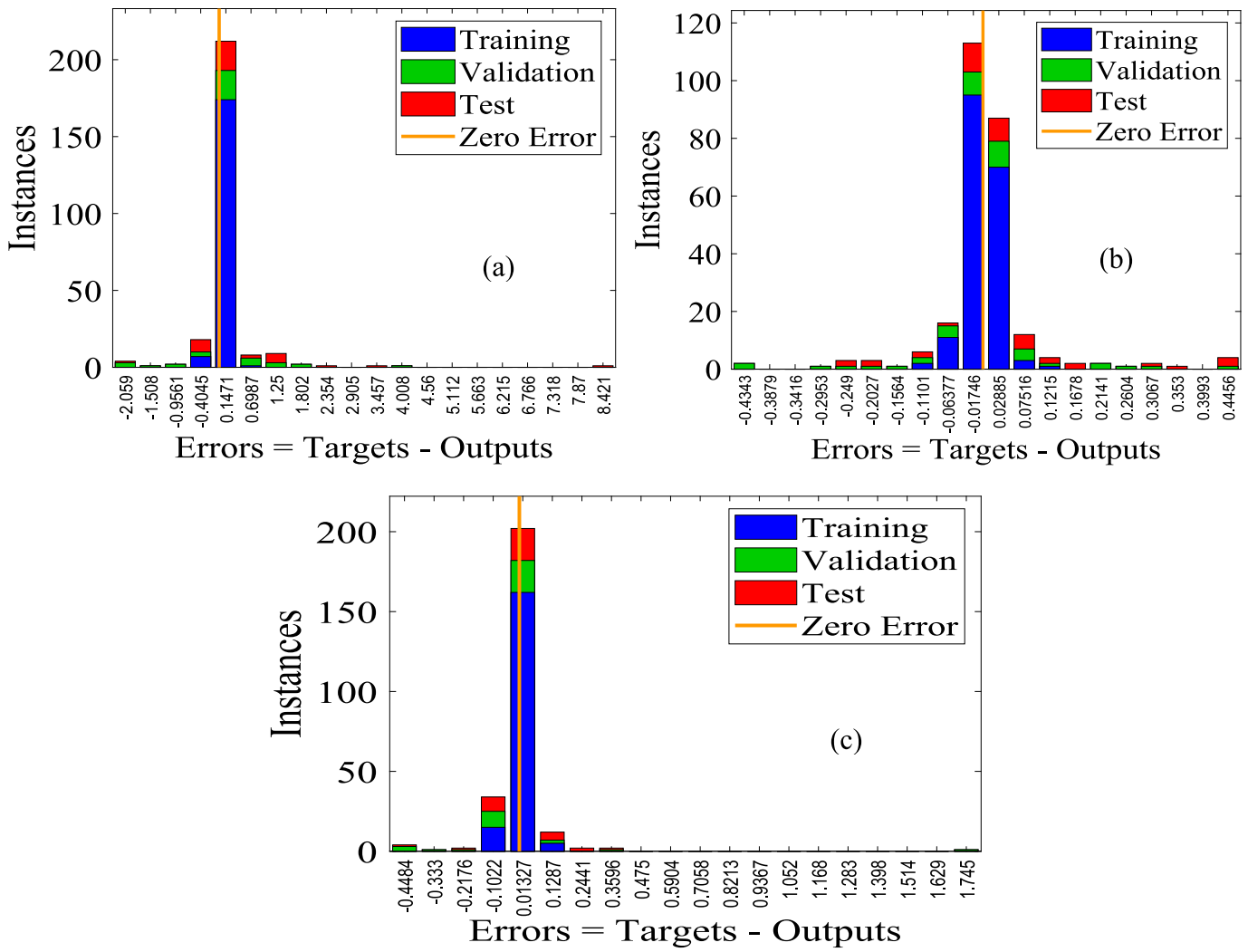

Fig. 15. Histogram errors for (a) compressive strength, (b) flexural strength, and (c) split tensile strength.

3.4. Performance indicators of network topology

Figs. 12 and 13 display the training effectiveness for each network architecture with 10-input layers, 3-hidden layer, and 2–20 neuron counts. The training process uses the Levenberg-Marquardt performance function of multiple perception neurons. Comparing the performance outputs from Figs. 12 and 13, the 10–20–20–20-1 network topology generated the best metrics for forecasting the compressive and flexural strengths of GPC modified with GGBFS and CCA. Whereas, 10–17–17–17-1 network structure gave the best performance metrics for predicting the split tensile strength. The results showed that the performance metrics improved as the number of neurons in the hidden layers increased, which is consistent with past research [139]. Comparing the best neuron count with the performance indices of greater and lower neuron counts, the mean squared error (MSE) performance for 20-neuron count was 56.52% and 99. 99% lower than 13 and 1 neuron counts in Fig. 12(a) and 14.29% and 99.66% lower than 18 and 1 neuron counts in Fig. 12(b), while MSE for 17-neuron count (the best for predicting split tensile strength) in Fig. 12(c) was 86.36% and 99.90% lower than 8 and 1 neuron counts, respectively. In the same vein, the corresponding regression coefficients (R) for training, validation, test, and all R were 99.99%, 99.53%, 98.91%, and 99.80% in Fig. 13(a), 99.96%, 98.24%, 98.11%, and 99.53% in Fig. 13(b), and 98.78%, 95.68%, 98.41%, and 98.30% in Fig. 13(c). Hence, Figs. 12 and 13 evidently signified that training, validating, and testing of GGBFS-CCA-GPC datasets using a 3-hidden layer with 20-neuron for compressive and flexural strengths and 3-hidden layer with 17-neuron in each layer for split tensile strength attained their best learning structures and yielded the best MSE and R. These metric results can be connected to several layers' generalization capabilities, which let them learn every feature between the input matrices and advanced categorization.

3.5. Validation of performance metrics for the best DNN topologies

Fig. 14 displays the best validation performance for the deep neural network structures engaging the Levenberg-Marquardt backpropagation training algorithm for multiple perception layers. The best validation performances gave 1.2864 at epoch 8, 0.029814 at epoch 6, and 0.11088 at epoch 7 for Figs. 14(a)–(c), respectively. Similarly, the error difference between the predicted and actual values are indicated in Fig. 15 with total error range divided into 20 smaller bins. Figs. 15(a)–(c) demonstrate bins corresponding to the errors of 0.1471, 0.005695, and 0.01327, respectively. For instance, the bin height lies to 170 for training datasets, and between 180 and 200 for validation and test datasets in Figs. 15(a) and (c), while the bin height lies to 90 for training datasets, and between 100 and 115 for validation and test datasets in Figs. 15(b). Hence, zero error points fell under the bin with centres 0.1471, 0.005695, and 0.01327 for Figs. 15(a)–(c). The assessment of strength and direction of linear relationships predicted and target variables are showed in Fig. 16. The combined correlation coefficients

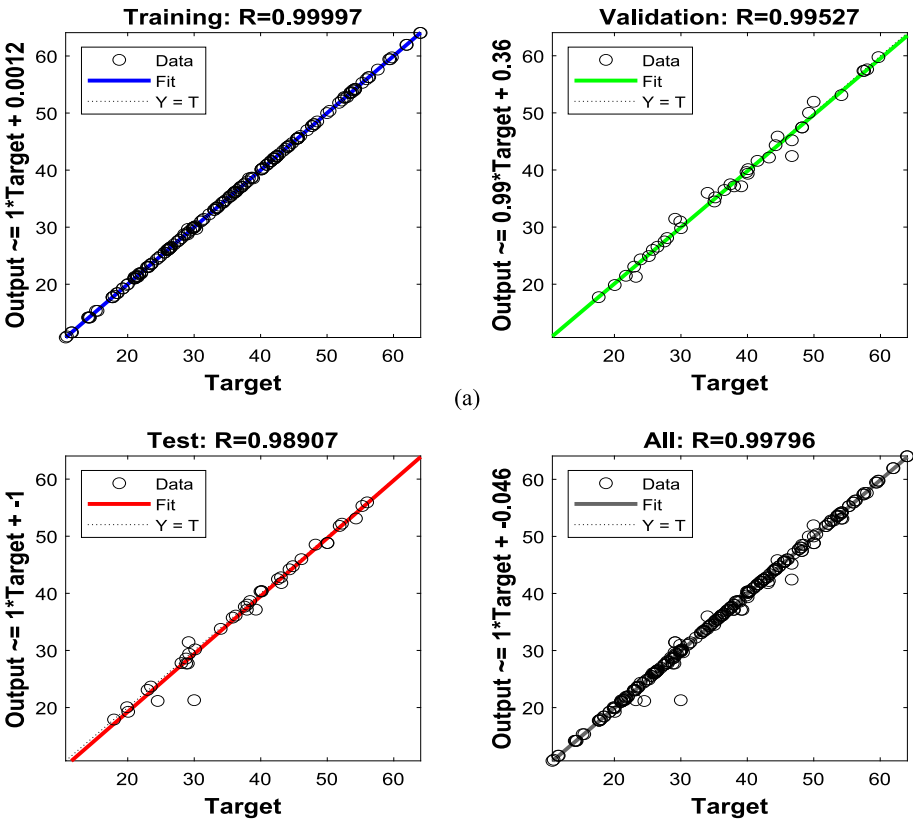

Fig. 16. Correlation coefficient outputs of the best deep neural network topology for (a) compressive strength, (b) flexural strength, and (c) split tensile strength.

revealed that the developed deep neural network can predict the compressive, flexural, and split tensile strengths with strong correlations 99.80%, 99.53%, and 97.57% at 95% confidence and predictive intervals for Figs. 16(a)–(c), respectively. According to the performance metrics mentioned above, R-values are approximately closer to 1 while MSE values were far from zero. These statistical outputs demonstrated the ability of the constructed deep neural network model to forecast the intended strengths (compressive, flexural, and split tensile strengths), resulting in correct precision and reduced error efficiency.

3.6. Validation of developed DNN models

It is essential to validate the accuracy and precision of any generated model using untrained datasets. In this regard, the untrained datasets generated from the experimental tests were used to validate the 10–20–20–20-1, which created the optimal network structure for forecasting CS and FS, and the 10–17–17–17-1 for forecasting STS. Table 5 provides information about the untrained datasets as well as the predicted values. Table 6 displays the absolute errors (AB) and relative error (RE) resulting from the correlation between the actual and predicted strengths. The magnitude of the difference between the actual and predicted values for compressive, flexural, and split tensile strengths and the percentage of error introduced during the prediction, as shown in Table 6, are absolute and percentage errors, respectively. About 18% of the datasets in Table 6 had absolute error over the zero line when predicting the compressive strength of GPC. The remaining 82% of the values demonstrated precise accuracy in comparing the magnitude between the actual and predicted strengths. This showed a strong correlation. However, there was no discernible difference between the actual and predicted flexural and split tensile strengths of the GPC generated. In addition, the predicted compressive strength, flexural strength, and split tensile strength of GGBFS-CCA-GPC with 10–20–20–20-1 and 10–17–17–17-1 network structures, as shown in Table 6, were within + 15.22% and −3.12%, +4.75% and −5.09%, and + 10.77% and −7.83%, respectively, for validating the developed deep neural networks. These findings support a related investigation in which the predicted compressive strengths of the GGBFS-fly ash-based GPC with the ANN model were within + 10% and −15% of the measured compressive strength for the training datasets. However, this value was increased to ± 20% for the other remaining models (LR, MLR, and M5P-tree) [71]. Another pertinent study revealed that the datasets of fly ash-based GPC had error lines of + 15% and −20% for the training data, +10% and −20% for the testing data, and + 15% and −10% for the validating datasets [72]. Ultimately, the deep neural network architectures created for forecasting the compressive, flexural, and split tensile strengths of the GPC modified with GGBFS and CCA are zero-efficient errors.

The relationship between the actual and predicted values were further analyzed and the results are shown in Fig. 17. The performance indexes revealed that a 10–20–20–20-1 deep neural network model developed for compressive and flexural strengths could accurately predict the input and output variables, yielding 98.61% R^2 for CS and 98.11% R^2 for FS. In the same vein, a 10–17–17–17-1 deep neural network model created for split tensile strength could forecast the strength's variables at 96.94% R^2. These performance indicators are in line with the outputs of the pertinent ANN model, which produced R^2 and RMSE values of 96.47% and 3.32 for training, 97.99% and 3.04 for testing, and 98.45% and 1.8381 for validating the correlation between the predicted and actual compressive strengths of fly ash-based concrete [72]. This is also consistent with the relationship between the predicted and actual compressive strengths of geopolymer concrete modified with fly ash and GGBFS; whose ANN model generated R^2 and RMSE of 98.81% and 2.478 for training, 99.46% and 2.15 for testing, and 99.79% and 0.9484 for validating the datasets [71]. These statistical results showed that the input and target arguments for the established network

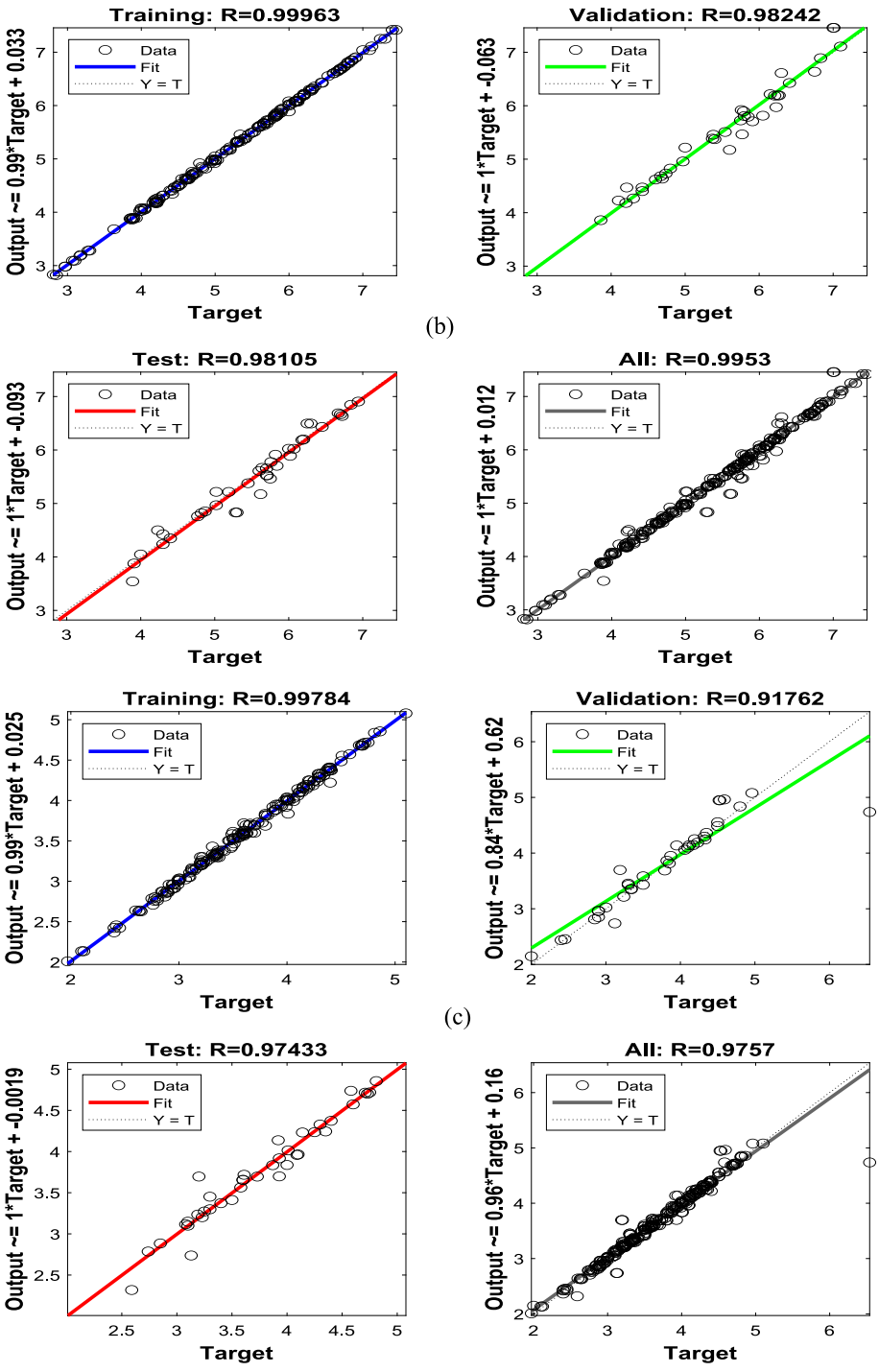

Fig. 16. (*continued*).

topologies had a high correlation. The strength prediction of GPC modified and synthesized with agro-industrial wastes and alkaline activating solutions under ambiently cured settings can ultimately be done using these deep neural network architectures.

4. Conclusions

This study applied the 3-hidden layer of deep neural networks with 2–20 neuron counts to predict the mechanical properties of GGBFS-CCA based-GPC synthesized with alkaline activating precursor at ambiently cured conditions. Ten different input variables from mix design proportions were used for the modeling, including GGBFS, CCA, FA, CA, W, SHP, SSG, CD, MC, and CG. The output arguments for the target were compressive strength, flexural strength, and split tensile strength. MSE and R were used to assess each neuron count's performance, and untrained datasets from the experiments were used to validate the generated models. These inferences can be drawn from the results obtained:

1. By employing GGBFS at 60% and CCA at 40% optimum as aluminosilicate precursors, geopolymer concrete with acceptable compressive, flexural, and split tensile strength values for structural applications could be produced.
2. The mechanical strengths of the GGBFS-CCA-GPC are significantly impacted by the GGBFS, concrete mix grade, curing days, and alkali

Table 5
Untrained statistics from experimental tests with actual and predicted values.

S/N	GGBFS	CCA	FA	CA	W	SHP	SSG	CD	MC	CG (kg/m^3)	Actual CS (MPa)	Pred. CS (MPa)	Actual FS (MPa)	Pred.FS (MPa)	Actual STS (MPa)	Pred. STS (MPa)
1	304	76	887	1045	37.86	20.74	146.4	7	12	30	26.25	26.44	4.77	4.62	2.98	3.01
2	228	152	874	1045	35.16	23.44	146.4	7	14	30	24.35	24.63	4.47	4.46	3.12	3.1
3	152	228	865	1045	32.64	25.96	146.4	7	16	30	18.13	17.98	3.89	3.85	2.82	2.83
4	380	0	899	1045	37.86	20.74	146.4	28	12	30	43.17	43.38	5.91	5.93	4.2	4.23
5	76	304	852	1045	35.16	23.44	146.4	28	14	30	27.11	26.99	4.43	4.41	3.19	3.2
6	0	380	841	1045	32.64	25.96	146.4	28	16	30	19.42	19.23	3.68	3.68	2.77	2.71
7	152	228	865	1045	37.86	20.74	146.4	56	12	30	28.85	29.04	4.98	5.05	3.53	3.47
8	228	152	874	1045	35.16	23.44	146.4	56	14	30	39.98	40.09	6.02	6	3.98	4.04
9	304	76	887	1045	35.16	23.44	146.4	56	14	30	44.12	43.75	6.2	6.22	4.2	4.25
10	152	228	865	1045	32.64	25.96	146.4	56	16	30	30.01	29.84	4.9	4.92	3.6	3.58
11	380	0	899	1045	37.86	20.74	146.4	90	12	30	46.77	45.2	6.25	6.19	4.35	4.31
12	228	152	874	1045	35.16	23.44	146.4	90	14	30	41.29	41.25	6	6.05	4.2	4.15
13	76	304	852	1045	32.64	25.96	146.4	90	16	30	24.49	21.16	4.25	4.42	3.19	3.23
14	390	98	788	1045	37.86	20.74	146.4	7	12	40	34.59	34.74	5.42	5.45	3.52	3.61
15	98	390	741	1045	32.64	23.44	146.4	7	14	40	23.13	19.67	4.34	4.42	2.93	2.73
16	98	390	741	1045	32.64	23.44	146.4	7	14	40	23.2	19.67	4.3	4.42	2.97	2.73
17	0	488	728	1045	32.64	25.96	146.4	7	16	40	18	17.91	3.91	3.54	2.6	2.32
18	390	98	788	1045	37.86	20.74	146.4	28	12	40	50.38	51.95	6.29	6.61	4.37	4.22
19	195	293	758	1045	35.16	23.44	146.4	28	14	40	42.77	42.48	5.88	5.95	3.65	3.71
20	390	98	788	1045	35.16	23.44	146.4	28	14	40	52.7	52.66	6.5	6.55	4.44	4.38
21	293	195	772	1045	32.64	25.96	146.4	28	16	40	46.7	42.44	6.2	5.97	4.02	4
22	0	488	728	1045	37.86	20.74	146.4	56	12	40	27.44	27.54	4.63	4.61	3.21	3.26
23	293	195	772	1045	35.16	23.44	146.4	56	14	40	50.4	50.39	6.4	6.4	4.4	4.37
24	488	0	805	1045	32.64	25.96	146.4	56	16	40	54.3	54.25	6.8	6.8	4.6	4.96
25	98	390	741	1045	37.86	20.74	146.4	90	12	40	38.69	38.69	5.66	5.66	3.91	3.7
26	195	293	758	1045	35.16	23.44	146.4	90	14	40	46.74	47	6.21	6.21	4.2	4.15
27	0	488	728	1045	35.16	23.44	146.4	90	14	40	32.19	32.26	5.13	5.1	3.69	3.69
28	195	293	758	1045	32.64	25.96	146.4	90	16	40	44.5	45.85	6.1	5.81	4	4.01

Table 6
Absolute and relative errors between the actual and predicted strengths.

S/N	Absolute error CS	FS	STS	Relative error (%) CS	FS	STS
1	−0.19	0.15	−0.03	−0.72	3.14	−1.01
2	−0.28	0.01	0.02	−1.15	0.22	0.64
3	0.15	0.04	−0.01	0.83	1.03	−0.35
4	−0.21	−0.02	−0.03	−0.49	−0.34	−0.71
5	0.12	0.02	−0.01	0.44	0.45	−0.31
6	0.19	0.00	0.06	0.98	0.00	2.17
7	−0.19	−0.07	0.06	−0.66	−1.41	1.70
8	−0.11	0.02	−0.06	−0.28	0.33	−1.51
9	0.37	−0.02	−0.05	0.84	−0.32	−1.19
10	0.17	−0.02	0.02	0.57	−0.41	0.56
11	1.57	0.06	0.04	3.36	0.96	0.92
12	0.04	−0.05	0.05	0.10	−0.83	1.19
13	3.33	−0.17	−0.04	13.60	−4.00	−1.25
14	−0.15	−0.03	−0.09	−0.43	−0.55	−2.56
15	3.46	−0.08	0.20	14.96	−1.84	6.83
16	3.53	−0.12	0.24	15.22	−2.79	8.08
17	0.09	0.37	0.28	0.50	9.46	10.77
18	−1.57	−0.32	0.15	−3.12	−5.09	3.43
19	0.29	−0.07	−0.06	0.68	−1.19	−1.64
20	0.04	−0.05	0.06	0.08	−0.77	1.35
21	4.26	0.23	0.02	9.12	3.71	0.50
22	−0.10	0.02	−0.05	−0.36	0.43	−1.56
23	0.01	0.00	0.03	0.02	0.00	0.68
24	0.05	0.00	−0.36	0.09	0.00	−7.83
25	0.00	0.00	0.21	0.00	0.00	5.37
26	−0.26	0.00	0.05	−0.56	0.00	1.19
27	−0.07	0.03	0.00	−0.22	0.58	0.00
28	−1.35	0.29	−0.01	−3.03	4.75	−0.25

precursors; however, the GGBFS provided the biggest significant contribution to the mechanical strengths with about 39% of the sensitivity factor.

3. 14 M Concentration of sodium hydroxide solution exhibited the best mechanical strengths compared to 12 M and 16 M
4. A 10–20–20–20-1 deep neural network structure gave the best performance indicators for predicting the compressive strength with 99.80% R and flexural strength 99.53% R compared to other network structures.
5. With a 10–17–17–17-1 deep neural network topology, the split tensile strength of the GGBFS-CCA-GPC could be predicted with the highest accuracy (97.57% R) compared to other network structures.
6. The evaluation and comparison of performance metrics (R^2 and MSE) for all training, testing, and validation datasets successfully confirmed the precision of the developed models.
7. The predicted compressive strength, flexural strength, and split tensile strength with the developed deep neural network model were within + 15.22% and −3.12%, +4.75% and −5.09%, and + 10.77% and 7.83% of the actual compressive, flexural, and split tensile strengths.
8. Strong correlation and precise precision are obtained when the developed deep neural network models are validated with untrained datasets, producing an R-value of appropriately 99%, 98%, and 97% for compressive, flexural, and split tensile strengths.

Using deep neural network techniques to forecast the strengths of GGBFS-CCA-based GPC can supplement the conventional empirical models by showing the prediction findings, more quickly and simply, enabling the concrete performance prediction with unknown mix proportions through deep neural network. This technique can help with timesaving, improved time efficiency, and theoretical and practical direction for optimizing concrete mix proportions. The research has demonstrated that the deep neural network can accurately predict the strengths despite the complexity and limitedness of the experimental data, and a concrete mix designer can utilize it as a new tool to help and enhance the decision-making process. It can also facilitate reductions in experimental effort, labor, and material consumption. Through these approaches, it will be easier to create and use sustainable concrete formulation that use different binding materials, including geopolymers, and have a smaller negative impact on the environment and operational expenses. Despite all of these advantages, it would be recommended to apply other AI approaches and a larger dataset containing data on the characteristics of the GPC's components to further enhance the models' performance.

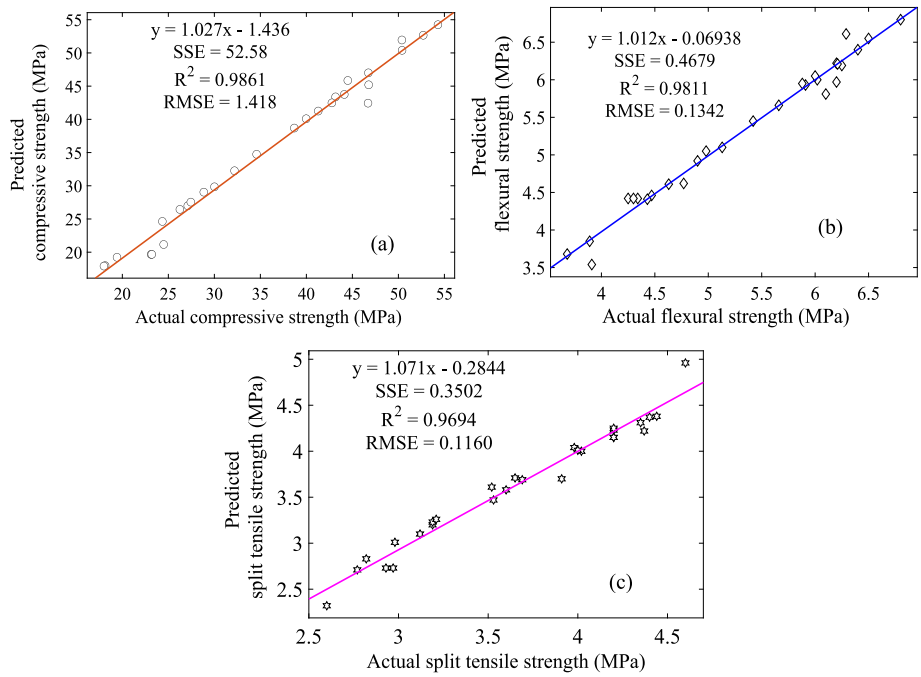

Fig. 17. Performance indicators for validating the relationship between the actual and predicted values for (a) compressive strength, (b) flexural strength, and (c) split tensile strength.

5. Data and code availability

Experimental data used in this study and code generation are available at https://github.com/Sotech281/AI-based-strength-prediction-of-geopolymer-concrete.

CRediT authorship contribution statement

Solomon Oyebisi: Conceptualization, Data curation, Formal analysis, Funding acquisition, Investigation, Software, Methodology, Writing – original draft. **Thamer Alomayri:** Funding acquisition, Project administration, Resources, Supervision, Validation, Writing – review & editing.

Declaration of Competing Interest

The authors declare that they have no known competing financial interests or personal relationships that could have appeared to influence the work reported in this paper.

Data availability

I have shared the link to my data/code at the attached file step

Acknowledgement

The authors thank Covenant University for providing a conducive atmosphere for this research.

References

[1] A. Ghosh, G.D. Ransinchung R.N., Application of machine learning algorithm to assess the efficacy of varying industrial wastes and curing methods on strength development of geopolymer concrete, Constr. Build. Mater. 341 (2022), 127828, https://doi.org/10.1016/j.conbuildmat.2022.127828.

[2] F. Belaïd, How does concrete and cement industry transformation contribute to mitigating climate change challenges? Resources, Conservation Recycling Adv. 15 (2022), 200084 https://doi.org/10.1016/j.rcradv.2022.200084.

[3] R.M. Andrew, Global CO₂ emissions from cement production, 1928–2018, Earth Syst. Sci. Data. 11 (2019) 1675–1710, https://doi.org/10.5194/essd-11-1675-2019.

[4] F. Puertas, J.A. Suárez-Navarro, M.M. Alonso, C. Gascó, NORM waste, cements, and concretes. A review, Mater. de Construcción. 71 (2021) e259.

[5] United States Environmental Protection Agency, United States Environmental Protection Agency, D.C., United States, Washington, 2008 https://www.epa.gov/coalash/coal-ash-basics (accessed October 20, 2022.

[6] T. Schaubroeck, T. Gibon, E. Igos, E. Benetto, Sustainability assessment of circular economy over time: modelling of finite and variable loops & impact distribution among related products, Resour. Conserv. Recycl. 168 (2021), 105319, https://doi.org/10.1016/j.resconrec.2020.105319.

[7] I.G. Shaaban, J.P. Rizzuto, A. El-Nemr, L. Bohan, H. Ahmed, H. Tindyebwa, Mechanical properties and air permeability of concrete containing waste tires extracts, J. Mater. Civ. Eng. 33 (2021), https://doi.org/10.1061/(ASCE)MT.1943-5533.0003588.

[8] et al. Nurruddin, Methods of curing geopolymer concrete: A review, International Journal of ADVANCED AND APPLIED SCIENCES. 5 (2018) 31–36. https://doi.org/10.21833/ijaas.2018.01.005.

[9] M.S. Saif, A.S. Shanour, G.E. Abdelaziz, H.I. Elsayad, I.G. Shaaban, B.A. Tayeh, M. S. Hammad, Influence of blended powders on properties of Ultra-High Strength Fibre Reinforced Self Compacting Concrete subjected to elevated temperatures, Case Stud. Constr. Mater. 18 (2023) e01793.

[10] H.M. Saleh, I.I. Bondouk, E. Salama, H.A. Esawii, Consistency and shielding efficiency of cement-bitumen composite for use as gamma-radiation shielding material, Prog. Nucl. Energy 137 (2021), 103764, https://doi.org/10.1016/j.pnucene.2021.103764.

[11] H.M. Saleh, I.I. Bondouk, E. Salama, H.H. Mahmoud, K. Omar, H.A. Esawii, Asphaltene or polyvinylchloride waste blended with cement to produce a sustainable material used in nuclear safety, Sustainability. 14 (2022) 3525, https://doi.org/10.3390/su14063525.

[12] S. Oyebisi, A. Ede, F. Olutoge, D. Omole, Geopolymer concrete incorporating agro-industrial wastes: effects on mechanical properties, microstructural behaviour and mineralogical phases, Constr. Build Mater. 256 (2020) 119390.

[13] S. Oyebisi, A. Ede, F. Olutoge, B. Ngene, Assessment of activity indexes on the splitting tensile strengthening of geopolymer concrete incorporating supplementary cementitious materials, Mater. Today Commun. 24 (2020) 101356.

[14] J. Davidovits, Geopolymers, J. Therm. Anal. 37 (1991) 1633–1656, https://doi.org/10.1007/BF01912193.

[15] G. Pazouki, Fly ash-based geopolymer concrete's compressive strength estimation by applying artificial intelligence methods, Measurement 203 (2022), 111916, https://doi.org/10.1016/j.measurement.2022.111916.

[16] J. He, Y. Jie, J. Zhang, Y. Yu, G. Zhang, Synthesis and characterization of red mud and rice husk ash-based geopolymer composites, Cem. Concr. Compos. 37 (2013) 108–118, https://doi.org/10.1016/j.cemconcomp.2012.11.010.

[17] Y. Peng, C. Unluer, Analyzing the mechanical performance of fly ash-based geopolymer concrete with different machine learning techniques, Constr. Build

Mater. 316 (2022), 125785, https://doi.org/10.1016/J.CONBUILDMAT.2021.125785.
[18] A.A. Shahmansouri, M. Yazdani, S. Ghanbari, H. Akbarzadeh Bengar, A. Jafari, H. Farrokh Ghatte, Artificial neural network model to predict the compressive strength of eco-friendly geopolymer concrete incorporating silica fume and natural zeolite, J. Clean Prod. 279 (2021), 123697, https://doi.org/10.1016/j.jclepro.2020.123697.
[19] W. Huo, Z. Zhu, H. Sun, B. Ma, L. Yang, Development of machine learning models for the prediction of the compressive strength of calcium-based geopolymers, J. Clean Prod. 380 (2022), 135159, https://doi.org/10.1016/J.JCLEPRO.2022.135159.
[20] B. Singh, G. Ishwarya, M. Gupta, S.K. Bhattacharyya, Geopolymer concrete: a review of some recent developments, Constr. Build Mater. 85 (2015) 78–90, https://doi.org/10.1016/j.conbuildmat.2015.03.036.
[21] B.P. Lenka, R.K. Majhi, S. Singh, A.N. Nayak, Eco-friendly and cost-effective concrete utilizing high-volume blast furnace slag and demolition waste with lime,, European J. Environ. Civil Eng. 26 (2022) 5351–5373, https://doi.org/10.1080/19648189.2021.1896581.
[22] R.K. Majhi, A.N. Nayak, Production of sustainable concrete utilising high-volume blast furnace slag and recycled aggregate with lime activator, J. Clean Prod. 255 (2020), 120188, https://doi.org/10.1016/j.jclepro.2020.120188.
[23] V. Revilla-Cuesta, V. Ortega-López, M. Skaf, A.-R. Khan, J.M. Manso, Deformational behavior of self-compacting concrete containing recycled aggregate, slag cement and green powders under compression and bending: description and prediction adjustment, J. Build. Eng. 54 (2022), 104611, https://doi.org/10.1016/j.jobe.2022.104611.
[24] V. Ortega-López, F. Faleschini, C. Pellegrino, V. Revilla-Cuesta, J.M. Manso, Validation of slag-binder fiber-reinforced self-compacting concrete with slag aggregate under field conditions: durability and real strength development, Constr. Build Mater. 320 (2022), 126280, https://doi.org/10.1016/j.conbuildmat.2021.126280.
[25] R.K. Majhi, A.N. Nayak, B.B. Mukharjee, Characterization of lime activated recycled aggregate concrete with high-volume ground granulated blast furnace slag, Constr. Build. Mater. 259 (2020), 119882, https://doi.org/10.1016/j.conbuildmat.2020.119882.
[26] W.P. Zakka, N.H. Abdul Shukor Lim, M.a. Chau Khun, A scientometric review of geopolymer concrete, J. Clean. Prod. 280 (2021), 124353, https://doi.org/10.1016/j.jclepro.2020.124353.
[27] P. Duxson, A. Fernández-Jiménez, J.L. Provis, G.C. Lukey, A. Palomo, J.S.J. van Deventer, Geopolymer technology: the current state of the art, J. Mater. Sci. 42 (2007) 2917–2933, https://doi.org/10.1007/s10853-006-0637-z.
[28] J.G.S. van Jaarsveld, J.S.J. van Deventer, Effect of the alkali metal activator on the properties of fly ash-based geopolymers, Ind. Eng. Chem. Res. 38 (1999) 3932–3941, https://doi.org/10.1021/ie980804b.
[29] H. Xu, J.S.J. van Deventer, The effect of alkali metals on the formation of geopolymeric gels from alkali-feldspars, Colloids Surf A Physicochem Eng Asp 216 (2003) 27–44, https://doi.org/10.1016/S0927-7757(02)00499-5.
[30] P. Duxson, S.W. Mallicoat, G.C. Lukey, W.M. Kriven, J.S.J. van Deventer, The effect of alkali and Si/Al ratio on the development of mechanical properties of metakaolin-based geopolymers, Colloids Surf A Physicochem Eng Asp 292 (2007) 8–20, https://doi.org/10.1016/j.colsurfa.2006.05.044.
[31] F. Farooq, X. Jin, M. Faisal Javed, A. Akbar, M. Izhar Shah, F. Aslam, R. Alyousef, Geopolymer concrete as sustainable material: a state of the art review, Constr. Build. Mater. 306 (2021), 124762, https://doi.org/10.1016/j.conbuildmat.2021.124762.
[32] M.N.S. Hadi, H. Zhang, S. Parkinson, Optimum mix design of geopolymer pastes and concretes cured in ambient condition based on compressive strength, setting time and workability, J. Build. Eng. 23 (2019) 301–313, https://doi.org/10.1016/j.jobe.2019.02.006.
[33] M.L. Kumar, V. Revathi, Microstructural properties of alkali-activated metakaolin and bottom ash geopolymer, Arab. J. Sci. Eng. 45 (2020) 4235–4246, https://doi.org/10.1007/s13369-020-04417-6.
[34] P. Kumar, C. Pankar, D. Manish, A.S. Santhi, Study of mechanical and microstructural properties of geopolymer concrete with GGBS and Metakaolin, Mater. Today:. Proc. 5 (2018) 28127–28135, https://doi.org/10.1016/j.matpr.2018.10.054.
[35] H.Q. Ahmed, D.K. Jaf, S.A. Yaseen, Flexural strength and failure of geopolymer concrete beams reinforced with carbon fibre-reinforced polymer bars, Constr. Build. Mater. 231 (2020), 117185, https://doi.org/10.1016/j.conbuildmat.2019.117185.
[36] F. Pelisser, B.V. Silva, M.H. Menger, B.J. Frasson, T.A. Keller, A.J. Torii, R. H. Lopez, Structural analysis of composite metakaolin-based geopolymer concrete, Revista IBRACON de Estruturas e Materiais. 11 (2018) 535–543, https://doi.org/10.1590/s1983-41952018000300006.
[37] W. Ferdous, A. Manalo, A. Khennane, O. Kayali, Geopolymer concrete-filled pultruded composite beams – concrete mix design and application, Cem. Concr. Compos. 58 (2015) 1–13, https://doi.org/10.1016/j.cemconcomp.2014.12.012.
[38] P. Nath, P.K. Sarker, Effect of GGBFS on setting, workability and early strength properties of fly ash geopolymer concrete cured in ambient condition, Constr. Build. Mater. 66 (2014) 163–171, https://doi.org/10.1016/j.conbuildmat.2014.05.080.
[39] K. Neupane, Fly ash and GGBFS based powder-activated geopolymer binders: A viable sustainable alternative of portland cement in concrete industry, Mech. Mater. 103 (2016) 110–122, https://doi.org/10.1016/j.mechmat.2016.09.012.
[40] N.S. Yacob, Shear behavior of reinforced fly ash-based geopolymer concrete, Missouri University of Science and Technology, Master, 2016.
[41] N.S. Yacob, M.A. ElGawady, L.H. Sneed, A. Said, Shear strength of fly ash-based geopolymer reinforced concrete beams, Eng. Struct. 196 (2019), 109298, https://doi.org/10.1016/j.engstruct.2019.109298.
[42] M.T. Ghafoor, Q.S. Khan, A.U. Qazi, M.N. Sheikh, M.N.S. Hadi, Influence of alkaline activators on the mechanical properties of fly ash based geopolymer concrete cured at ambient temperature, Constr. Build. Mater. 273 (2021), 121752, https://doi.org/10.1016/j.conbuildmat.2020.121752.
[43] N.A. Farhan, M.N. Sheikh, M.N.S. Hadi, Investigation of engineering properties of normal and high strength fly ash based geopolymer and alkali-activated slag concrete compared to ordinary Portland cement concrete, Constr. Build. Mater. 196 (2019) 26–42, https://doi.org/10.1016/j.conbuildmat.2018.11.083.
[44] M.A.M. Ariffin, M.A.R. Bhutta, M.W. Hussin, M. Mohd Tahir, N. Aziah, Sulfuric acid resistance of blended ash geopolymer concrete, Constr. Build. Mater. 43 (2013) 80–86, https://doi.org/10.1016/j.conbuildmat.2013.01.018.
[45] T. Bakharev, J.G. Sanjayan, Y.-B. Cheng, Resistance of alkali-activated slag concrete to acid attack, Cem. Concr. Res. 33 (2003) 1607–1611, https://doi.org/10.1016/S0008-8846(03)00125-X.
[46] K.-H. Yang, J.-K. Song, Workability loss and compressive strength development of cementless mortars activated by combination of sodium silicate and sodium hydroxide, J. Mater. Civ. Eng. 21 (2009) 119–127, https://doi.org/10.1061/(ASCE)0899-1561(2009)21:3(119).
[47] M.C.N.J.K.D.N.L. and D.S. N.P. Rajamane, Sulphate resistance and eco-friendliness of geopolymer concretes, Indian Concrete Journal. 86 (2012) 13–22.
[48] S.A. Bernal, R. Mejía de Gutiérrez, J.L. Provis, Engineering and durability properties of concretes based on alkali-activated granulated blast furnace slag/metakaolin blends, Constr. Build. Mater. 33 (2012) 99–108, https://doi.org/10.1016/j.conbuildmat.2012.01.017.
[49] M. Olivia, H. Nikraz, Properties of fly ash geopolymer concrete designed by Taguchi method, Mater. Design (1980-2015) 36 (2012) 191–198.
[50] D. Reddy, Experimental evaluation of the durability of fly ash-based geopolymer concrete in the marine environment, Mater. Sci. Eng. (2011).
[51] H.U. Ahmed, A.A. Mohammed, A.S. Mohammed, Effectiveness of silicon dioxide nanoparticles (nano sio2) on the internal structures, electrical conductivity, and elevated temperature behaviors of geopolymer concrete composites, J. Inorg. Organomet. Polym Mater. (2023), https://doi.org/10.1007/s10904-023-02672-2.
[52] H.U. Ahmed, A.S. Mohammed, A.A. Mohammed, Engineering properties of geopolymer concrete composites incorporated recycled plastic aggregates modified with nano-silica, J. Build. Eng. 75 (2023), 106942, https://doi.org/10.1016/j.jobe.2023.106942.
[53] H.U. Ahmed, A.A. Mohammed, A.S. Mohammed, Effectiveness of nano-SiO2 on the mechanical, durability, and microstructural behavior of geopolymer concrete at different curing ages, Archives of Civil Mech. Eng. 23 (2023) 129, https://doi.org/10.1007/s43452-023-00668-w.
[54] O. Avci, O. Abdeljaber, S. Kiranyaz, M. Hussein, M. Gabbouj, D.J. Inman, A review of vibration-based damage detection in civil structures: from traditional methods to machine learning and deep learning applications, Mech. Syst. Sig. Process. 147 (2021), 107077, https://doi.org/10.1016/j.ymssp.2020.107077.
[55] Z. Ghahramani, Probabilistic machine learning and artificial intelligence, Nature 521 (2015) 452–459, https://doi.org/10.1038/nature14541.
[56] Summary for Policymakers, in: Climate Change 2013 – The Physical Science Basis, Cambridge University Press, 2014: pp. 1–30. https://doi.org/10.1017/CBO9781107415324.004.
[57] T.G. Dietterich, Ensemble Methods in Machine Learning, in: 2000: pp. 1–15. https://doi.org/10.1007/3-540-45014-9_1.
[58] M. Haenlein, A. Kaplan, A brief history of artificial intelligence: on the past, present, and future of artificial intelligence, Calif. Manage. Rev. 61 (2019) 5–14, https://doi.org/10.1177/0008125619864925.
[59] A. Marani, M.L. Nehdi, Machine learning prediction of compressive strength for phase change materials integrated cementitious composites, Constr. Build. Mater. 265 (2020), 120286, https://doi.org/10.1016/j.conbuildmat.2020.120286.
[60] A. Ahmad, W. Ahmad, F. Aslam, P. Joyklad, Compressive strength prediction of fly ash-based geopolymer concrete via advanced machine learning techniques, Case Stud. Constr. Mater. 16 (2022) e00840.
[61] M. Timur Cihan, Prediction of concrete compressive strength and slump by machine learning methods, Adv. Civil Eng. 2019 (2019) 1–11.
[62] A. Raza, Q.u.Z. Khan, A. Ahmad, Prediction of axial compressive strength for frp-confined concrete compression members, KSCE J. Civ. Eng. 24 (7) (2020) 2099–2109.
[63] M.Y. Mansour, M. Dicleli, J.Y. Lee, J. Zhang, Predicting the shear strength of reinforced concrete beams using artificial neural networks, Eng. Struct. 26 (2004) 781–799, https://doi.org/10.1016/j.engstruct.2004.01.011.
[64] A.K. Tamimi, J.A. Abdalla, Z.I. Sakka, Prediction of long term chloride diffusion of concrete in harsh environment, Constr. Build. Mater. 22 (2008) 829–836, https://doi.org/10.1016/j.conbuildmat.2007.01.001.
[65] S. Nazar, J. Yang, A. Ahmad, S.F.A. Shah, Comparative study of evolutionary artificial intelligence approaches to predict the rheological properties of fresh concrete, Mater. Today Commun. 32 (2022), 103964, https://doi.org/10.1016/j.mtcomm.2022.103964.
[66] H. Song, A. Ahmad, F. Farooq, K.A. Ostrowski, M. Maślak, S. Czarnecki, F. Aslam, Predicting the compressive strength of concrete with fly ash admixture using machine learning algorithms, Constr. Build. Mater. 308 (2021), 125021, https://doi.org/10.1016/j.conbuildmat.2021.125021.
[67] M. Mohtasham Moein, A. Saradar, K. Rahmati, S.H. Ghasemzadeh Mousavinejad, J. Bristow, V. Aramali, M. Karakouzian, Predictive models for concrete properties

using machine learning and deep learning approaches: a review, J. Build. Eng. 63 (2023), 105444, https://doi.org/10.1016/j.jobe.2022.105444.
[68] H. Unis Ahmed, A.S. Mohammed, A.A. Mohammed, Fresh and mechanical performances of recycled plastic aggregate geopolymer concrete modified with Nano-silica: experimental and computational investigation, Constr. Build. Mater. 394 (2023), 132266, https://doi.org/10.1016/j.conbuildmat.2023.132266.
[69] H.U. Ahmed, A.S. Mohammed, R.H. Faraj, A.A. Abdalla, S.M.A. Qaidi, N.H. Sor, A.A. Mohammed, Innovative modeling techniques including MEP, ANN and FQ to forecast the compressive strength of geopolymer concrete modified with nanoparticles, Neural Comput Appl. 35 (2023) 12453–12479, https://doi.org/10.1007/s00521-023-08378-3.
[70] H.U. Ahmed, R.R. Mostafa, A. Mohammed, P. Sihag, A. Qadir, Support vector regression (SVR) and grey wolf optimization (GWO) to predict the compressive strength of GGBFS-based geopolymer concrete, Neural Comput. & Applic. 35 (2023) 2909–2926, https://doi.org/10.1007/s00521-022-07724-1.
[71] H.U. Ahmed, A.A. Mohammed, A. Mohammed, T. Xie, Soft computing models to predict the compressive strength of GGBS/FA- geopolymer concrete, PLoS One 17 (5) (2022) e0265846.
[72] H.U. Ahmed, A.S. Mohammed, S.M.A. Qaidi, R.H. Faraj, N. Hamah Sor, A. A. Mohammed, Compressive strength of geopolymer concrete composites: a systematic comprehensive review, analysis and modeling, Eur. J. Environ. Civ. Eng. 27 (2023) 1383–1428, https://doi.org/10.1080/19648189.2022.2083022.
[73] L. Deng, Deep Learning: Methods and Applications, Foundations and Trends® in Signal Processing. 7 (2014) 197–387. https://doi.org/10.1561/2000000039.
[74] Y. Bengio, Learning deep architectures for ai, foundations and trends® in machine, Learning 2 (2009) 1–127, https://doi.org/10.1561/2200000006.
[75] J. Schmidhuber, Deep learning in neural networks: an overview, Neural Netw. 61 (2015) 85–117, https://doi.org/10.1016/j.neunet.2014.09.003.
[76] B.A. Omran, Q. Chen, R. Jin, Comparison of data mining techniques for predicting compressive strength of environmentally friendly concrete, J. Comput. Civ. Eng. 30 (2016), https://doi.org/10.1061/(ASCE)CP.1943-5487.0000596.
[77] C. Bilim, C.D. Atiş, H. Tanyildizi, O. Karahan, Predicting the compressive strength of ground granulated blast furnace slag concrete using artificial neural network, Adv. Eng. Softw. 40 (2009) 334–340, https://doi.org/10.1016/j.advengsoft.2008.05.005.
[78] E.M. Golafshani, A. Behnood, M. Arashpour, Predicting the compressive strength of normal and high-performance concretes using ann and anfis hybridized with grey wolf optimizer, Constr. Build. Mater. 232 (2020), 117266, https://doi.org/10.1016/J.CONBUILDMAT.2019.117266.
[79] D. Dao, H.-B. Ly, S. Trinh, T.-T. Le, B. Pham, Artificial intelligence approaches for prediction of compressive strength of geopolymer concrete, Materials. 12 (2019) 983, https://doi.org/10.3390/ma12060983.
[80] C. Deepa, K. SathiyaKumari, V.P. Sudha, Prediction of the compressive strength of high performance concrete mix using tree based modeling, Int. J. Comput. Appl. 6 (2010) 18–24, https://doi.org/10.5120/1076-1406.
[81] D.-K. Bui, T. Nguyen, J.-S. Chou, H. Nguyen-Xuan, T.D. Ngo, A modified firefly algorithm-artificial neural network expert system for predicting compressive and tensile strength of high-performance concrete, Constr. Build. Mater. 180 (2018) 320–333, https://doi.org/10.1016/j.conbuildmat.2018.05.201.
[82] A.S.M. Mohammad Mohtasham, Predicting the compressive strength of alkali-activated concrete using various data mining methods, in: Proceedings of the Canadian Society of Civil Engineering Annual Conference 2021, Springer Nature Singapore, Singapore, 2022.
[83] A.F. Kocamaz, Y. Ayaz, M.B. Karakoç, İ. Türkmen, R. Demirboğa, Prediction of compressive strength and ultrasonic pulse velocity of admixtured concrete using tree model M5P, Struct. Concr. 22 (2021), https://doi.org/10.1002/suco.202000061.
[84] Q. Han, C. Gui, J. Xu, G. Lacidogna, A generalized method to predict the compressive strength of high-performance concrete by improved random forest algorithm, Constr. Build. Mater. 226 (2019) 734–742, https://doi.org/10.1016/j.conbuildmat.2019.07.315.
[85] J.-S. Chou, C.-K. Chiu, M. Farfoura, I. Al-Taharwa, Optimizing the prediction accuracy of concrete compressive strength based on a comparison of data-mining techniques, J. Comput. Civ. Eng. 25 (2011) 242–253, https://doi.org/10.1061/(ASCE)CP.1943-5487.0000088.
[86] M.-Y. Cheng, P.M. Firdausi, D. Prayogo, High-performance concrete compressive strength prediction using Genetic Weighted Pyramid Operation Tree (GWPOT), Eng. Appl. Artif. Intel. 29 (2014) 104–113, https://doi.org/10.1016/j.engappai.2013.11.014.
[87] P.R.V.M. Prem, Applied linear and nonlinear statistical models for evaluating strength of Geopolymer concrete, Comput. Concr. 24 (2019) 7–17.
[88] A. Nazari, J.G. Sanjayan, Modelling of compressive strength of geopolymer paste, mortar and concrete by optimized support vector machine, Ceram. Int. 41 (2015) 12164–12177, https://doi.org/10.1016/j.ceramint.2015.06.037.
[89] M.-Y. Cheng, J.-S. Chou, A.F.V. Roy, Y.-W. Wu, High-performance concrete compressive strength prediction using time-weighted evolutionary fuzzy support vector machines inference model, Autom. Constr. 28 (2012) 106–115, https://doi.org/10.1016/j.autcon.2012.07.004.
[90] A.-D. Pham, N.-D. Hoang, Q.-T. Nguyen, predicting compressive strength of high-performance concrete using metaheuristic-optimized least squares support vector regression, J. Comput. Civ. Eng. 30 (2016), https://doi.org/10.1061/(ASCE)CP.1943-5487.0000506.
[91] Y. Yu, W. Li, J. Li, T.N. Nguyen, A novel optimised self-learning method for compressive strength prediction of high performance concrete, Constr. Build. Mater. 184 (2018) 229–247, https://doi.org/10.1016/j.conbuildmat.2018.06.219.
[92] A. Ahmad, F. Farooq, P. Niewiadomski, K. Ostrowski, A. Akbar, F. Aslam, R. Alyousef, Prediction of compressive strength of fly ash based concrete using individual and ensemble algorithm, Materials. 14 (2021) 794, https://doi.org/10.3390/ma14040794.
[93] F. Farooq, W. Ahmed, A. Akbar, F. Aslam, R. Alyousef, Predictive modeling for sustainable high-performance concrete from industrial wastes: a comparison and optimization of models using ensemble learners, J. Clean. Prod. 292 (2021), 126032, https://doi.org/10.1016/j.jclepro.2021.126032.
[94] M. Azimi-Pour, H. Eskandari-Naddaf, A. Pakzad, Linear and non-linear SVM prediction for fresh properties and compressive strength of high volume fly ash self-compacting concrete, Constr. Build. Mater. 230 (2020), 117021, https://doi.org/10.1016/j.conbuildmat.2019.117021.
[95] P. Saha, P. Debnath, P. Thomas, Prediction of fresh and hardened properties of self-compacting concrete using support vector regression approach, Neural Comput. & Applic. 32 (2020) 7995–8010, https://doi.org/10.1007/s00521-019-04267-w.
[96] F. Aslam, F. Farooq, M.N. Amin, K. Khan, A. Waheed, A. Akbar, M.F. Javed, R. Alyousef, H. Alabdulijabbar, Applications of gene expression programming for estimating compressive strength of high-strength concrete, Adv. Civil Eng. 2020 (2020) 1–23, https://doi.org/10.1155/2020/8850535.
[97] F. Farooq, M. Nasir Amin, K. Khan, M. Rehan Sadiq, M.F. Faisal Javed, F. Aslam, R. Alyousef, A comparative study of random forest and genetic engineering programming for the prediction of compressive strength of high strength concrete (HSC), Appl. Sci. 10 (2020) 7330, https://doi.org/10.3390/app10207330.
[98] P.G. Asteris, K.G. Kolovos, Self-compacting concrete strength prediction using surrogate models, Neural Comput. Applic. 31 (2019) 409–424, https://doi.org/10.1007/s00521-017-3007-7.
[99] M. Sarıdemir, Genetic programming approach for prediction of compressive strength of concretes containing rice husk ash, Constr. Build. Mater. 24 (2010) 1911–1919, https://doi.org/10.1016/j.conbuildmat.2010.04.011.
[100] E.M. Golafshani, A. Behnood, Estimating the optimal mix design of silica fume concrete using biogeography-based programming, Cem. Concr. Compos. 96 (2019) 95–105, https://doi.org/10.1016/j.cemconcomp.2018.11.005.
[101] M.F. Javed, M.N. Amin, M.I. Shah, K. Khan, B. Iftikhar, F. Farooq, F. Aslam, R. Alyousef, H. Alabduljabbar, Applications of gene expression programming and regression techniques for estimating compressive strength of bagasse ash based concrete, Crystals (Basel). 10 (2020) 737, https://doi.org/10.3390/cryst10090737.
[102] D. Dao, S. Trinh, H.-B. Ly, B. Pham, Prediction of compressive strength of geopolymer concrete using entirely steel slag aggregates: novel hybrid artificial intelligence approaches, Appl. Sci. 9 (2019) 1113, https://doi.org/10.3390/app9061113.
[103] P.O. Awoyera, M.S. Kirgiz, A. Viloria, D. Ovallos-Gazabon, Estimating strength properties of geopolymer self-compacting concrete using machine learning techniques, J. Mater. Res. Technol. 9 (2020) 9016–9028, https://doi.org/10.1016/j.jmrt.2020.06.008.
[104] British Standard EN 196- 3, Method of Testing Cement: Physical Test, London, 2016.
[105] British Standard EN 196-6, Methods of Testing Cement: Determination of Fineness, London, 2018.
[106] S.U. Khan, M.F. Nuruddin, T. Ayub, N. Shafiq, Effects of different mineral admixtures on the properties of fresh concrete, Sci. World J. 2014 (2014) 1–11, https://doi.org/10.1155/2014/986567.
[107] British Standard EN 12620, Aggregates from Natural Sources for Concrete, London, 2013.
[108] American Concrete Institute 211-1, Standard Practice for Selecting Proportions for Normal, Heavyweight, and Mass Concrete, USA, 2002.
[109] M. Indhumathi Anbarasan, S.R. Sanjaiyan, S. Nagan Soundarapandiyan, Advances in Geopolymer-Zeolite Composites - Synthesis and Characterization, IntechOpen, 2021.
[110] S. Oyebisi, F. Olutoge, P. Kathirvel, I. Oyaotuderekumor, D. Lawanson, J. Nwani, A. Ede, R. Kaze, Sustainability assessment of geopolymer concrete synthesized by slag and corncob ash, Case Stud. Constr. Mater. 17 (2022) e01665.
[111] A. Noushini, A. Castel, J. Aldred, A. Rawal, Chloride diffusion resistance and chloride binding capacity of fly ash-based geopolymer concrete, Cem. Concr. Compos. 105 (2020), 103290, https://doi.org/10.1016/j.cemconcomp.2019.04.006.
[112] R.J.N.P. Rajamane, Quantities of sodium hydroxide solids and water to prepare sodium hydroxide solution of given molarity for geopolymer concrete mixes, India (2014).
[113] British Standard EN 12390- 4, Testing Hardened Concrete: Compressive Strength of Test Specimens, London, 2019.
[114] British Standard EN 12390-5, Testing Hardened Concrete: Flexural Strength of Test Specimens, London, 2019.
[115] British Standard EN 12390-6, Testing Hardened Concrete: Splitting Tensile Strength of Test Specimens, London, 2019.
[116] H.B.D.M.H.B.O.D.J. Martin T. Hagan, Neural Network Design, 2nd ed., Martin Hagan, Oklahoma, 2014.
[117] G. Panchal, A. Ganatra, Y.P. Kosta, D. Panchal, Behaviour analysis of multilayer perceptronswith multiple hidden neurons and hidden layers, Int. J. Computer Theory Eng.. (2011) 332–337, https://doi.org/10.7763/IJCTE.2011.V3.328.
[118] M. Uzair, N. Jamil, Effects of Hidden Layers on the Efficiency of Neural networks, in:2020 IEEE 23rd International Multitopic Conference (INMIC), IEEE (2020) 1–6, https://doi.org/10.1109/INMIC50486.2020.9318195.
[119] H.-B. Ly, T.-A. Nguyen, H.-V. Thi Mai, V.Q. Tran, Development of deep neural network model to predict the compressive strength of rubber concrete, Constr.

Build. Mater. 301 (2021), 124081, https://doi.org/10.1016/j.conbuildmat.2021.124081.
[120] H.U. Ahmed, A.A. Mohammed, A.S. Mohammed, The role of nanomaterials in geopolymer concrete composites: a state-of-the-art review, J. Build. Eng. 49 (2022), 104062, https://doi.org/10.1016/j.jobe.2022.104062.
[121] H. Unis Ahmed, L.J. Mahmood, M.A. Muhammad, R.H. Faraj, S.M.A. Qaidi, N. Hamah Sor, A.S. Mohammed, A.A. Mohammed, Geopolymer concrete as a cleaner construction material: an overview on materials and structural performances, Cleaner Materials. 5 (2022), 100111, https://doi.org/10.1016/j.clema.2022.100111.
[122] 96/04917 The influence of high early-strength (HES) mineralized clinker on the strength of development of blended cements containing fly ash, slag, or ground limestone, Fuel and Energy Abstracts. 37 (1996) 347. https://doi.org/10.1016/0140-6701(96)89649-4.
[123] S. Nagajothi, S. Elavenil, Effect of GGBS addition on reactivity and microstructure properties of ambient cured fly ash based geopolymer concrete, SILICON 13 (2021) 507–516, https://doi.org/10.1007/s12633-020-00470-w.
[124] K. Ganesh Babu, V. Sree Rama Kumar, Efficiency of GGBS in concrete, Cem. Concr. Res. 30 (2000) 1031–1036, https://doi.org/10.1016/S0008-8846(00)00271-4.
[125] K.M. Haneefa, M. Santhanam, F.C. Parida, Performance characterization of geopolymer composites for hot sodium exposed sacrificial layer in fast breeder reactors, Nucl. Eng. Des. 265 (2013) 542–553, https://doi.org/10.1016/j.nucengdes.2013.09.004.
[126] S. Kumar, R. Kumar, S.P. Mehrotra, Influence of granulated blast furnace slag on the reaction, structure and properties of fly ash based geopolymer, J. Mater. Sci. 45 (2010) 607–615, https://doi.org/10.1007/s10853-009-3934-5.
[127] T. Phoo-ngernkham, A. Maegawa, N. Mishima, S. Hatanaka, P. Chindaprasirt, Effects of sodium hydroxide and sodium silicate solutions on compressive and shear bond strengths of FA–GBFS geopolymer, Constr. Build. Mater. 91 (2015) 1–8, https://doi.org/10.1016/j.conbuildmat.2015.05.001.
[128] S. Naskar, A.K. Chakraborty, Effect of nano materials in geopolymer concrete, Perspect. Sci. (Neth). 8 (2016) 273–275, https://doi.org/10.1016/j.pisc.2016.04.049.
[129] B. Joseph, G. Mathew, Influence of aggregate content on the behavior of fly ash based geopolymer concrete, Sci. Iran. 19 (2012) 1188–1194, https://doi.org/10.1016/j.scient.2012.07.006.
[130] A. Hassan, M. Arif, M. Shariq, Use of geopolymer concrete for a cleaner and sustainable environment – a review of mechanical properties and microstructure, J. Clean. Prod. 223 (2019) 704–728, https://doi.org/10.1016/j.jclepro.2019.03.051.
[131] H.-B. Le, Q.-B. Bui, L. Tang, Geopolymer recycled aggregate concrete: from experiments to empirical models, Materials. 14 (2021) 1180, https://doi.org/10.3390/ma14051180.
[132] P. Posi, C. Teerachanwit, C. Tanutong, S. Limkamoltip, S. Lertnimoolchai, V. Sata, P. Chindaprasirt, Lightweight geopolymer concrete containing aggregate from recycle lightweight block, Mater. Design (1980-2015) 52 (2013) 580–586.
[133] P. Nuaklong, V. Sata, P. Chindaprasirt, Influence of recycled aggregate on fly ash geopolymer concrete properties, J. Clean. Prod. 112 (2016) 2300–2307, https://doi.org/10.1016/j.jclepro.2015.10.109.
[134] E. Vasconcelos, S. Fernandes, B. de Aguiar, F. Pacheco-Torgal, Concrete retrofitting using cfrp and geopolymer mortars, Mater. Sci. Forum 730–732 (2012) 427–432, https://doi.org/10.4028/www.scientific.net/MSF.730-732.427.
[135] S.J. Chithambaram, S. Kumar, M.M. Prasad, D. Adak, Effect of parameters on the compressive strength of fly ash based geopolymer concrete, Struct. Concr. 19 (2018) 1202–1209, https://doi.org/10.1002/suco.201700235.
[136] A.A. Aliabdo, A.E.M. Abd Elmoaty, H.A. Salem, Effect of water addition, plasticizer and alkaline solution constitution on fly ash based geopolymer concrete performance, Constr. Build. Mater. 121 (2016) 694–703, https://doi.org/10.1016/j.conbuildmat.2016.06.062.
[137] P.R. Vora, U.V. Dave, Parametric studies on compressive strength of geopolymer concrete, Procedia Eng. 51 (2013) 210–219, https://doi.org/10.1016/j.proeng.2013.01.030.
[138] A.T. Huynh, Q.D. Nguyen, Q.L. Xuan, B. Magee, T. Chung, K.T. Tran, K.T. Nguyen, A Machine learning-assisted numerical predictor for compressive strength of geopolymer concrete based on experimental data and sensitivity analysis, Appl. Sci. 10 (2020) 7726, https://doi.org/10.3390/app10217726.
[139] I. Shafi, J. Ahmad, S.I. Shah, F.M. Kashif, Impact of varying neurons and hidden layers in neural network architecture for a time frequency application, in: 2006 ieee international multitopic conference, IEEE 2006 (2006) 188–193, https://doi.org/10.1109/INMIC.2006.358160.